Coupled thermo-hydro-chemical modeling of accelerated carbonation of cementbased materials: application to CO 2 uptake

Farah Kaddah, Ouali Amiri, Philippe Turcry, Harifidy Ranaivomanana, Emmanuel Roziere

Coupled thermo-hydro-chemical modeling of accelerated carbonation of cement-based materials: application to CO_2 uptake

Farah Kaddah, Ouali Amiri, Philippe Turcry, Harifidy Ranaivomanana, Emmanuel Roziere

PII: S2352-7102(24)01387-1

DOI: https://doi.org/10.1016/j.jobe.2024.109819

Reference: JOBE 109819

To appear in: *Journal of Building Engineering*

Received Date: 2 January 2024

Revised Date: 31 May 2024

Accepted Date: 2 June 2024

Please cite this article as: F. Kaddah, O. Amiri, P. Turcry, H. Ranaivomanana, E. Roziere, Coupled thermo-hydro-chemical modeling of accelerated carbonation of cement-based materials: application to CO_2 uptake, *Journal of Building Engineering*, https://doi.org/10.1016/j.jobe.2024.109819.

Coupled thermo-hydro-chemical modeling of accelerated carbonation of cement-based materials: application to CO_2 uptake

Farah Kaddah [a c], Ouali Amiri [a], Philippe Turcry [b], Harifidy Ranaivomanana [a], Emmanuel Roziere [c]

[a] Nantes Université, CNRS, GeM, UMR 6183, F-44000 Nantes, France

[b] La Rochelle University, LaSIE UMR CNRS 7356, Avenue Michel Crepeau, 17042, La Rochelle Cedex 1, France

[c] Ecole Centrale de Nantes, 1 rue de la Noe – 44321 Nantes, France

Abstract

The use of CO_2-rich hot gases from cement plants or combustion processes is considered as an attractive method to accelerate the carbonation of recycled concrete aggregates (RCA). However, there is limited knowledge regarding the kinetics and mechanisms of accelerated carbonation induced by wet gas with a temperature of approximately 80°C. Water transport and temperature influence several parameters of the carbonation of cement-based materials, thus understanding and predicting their overall effect remains complex. The present study combines experimental and numerical investigations into the effects of temperature on carbonation processes. The experimental study focuses on understanding the effects of temperature on the evolution of the carbonation front, changes in chemical composition, and moisture transport within a cement-based material during carbonation in controlled conditions. The experimental data obtained serve as calibration parameters for a thermo-hydro-chemical coupled model of carbonation. The carbonation model incorporates heat transfer between the cement-based material and the external environment, considering the influence of temperature on water transfer, as well as the dissolution and carbonation of hydration products.

Keywords: Recycled concrete aggregates, Carbonation, Carbon Capture and Utilization (CCU), Temperature, CO_2, Water transport

Nomenclature

C_P heat capacity of the cementitious material (J.kg^{-1} .K^{-1})
C_{pv} thermal capacity of the gas mixture (J.kg^{-1} .K^{-1})
D_{CO2} coefficient of diffusion for gaseous CO_2 (m^2/s)
$D^0_{CO_2}$ diffusion coefficient of carbon dioxide in the air at 25°C (m^2/s)
D_{va} diffusion coefficient of water vapor in the air (m^2/s)
E_a: activation energy (J/mol)
J_c molar flux of carbon dioxide (kg/m^2/s^1)
J_V density of the mass flow of vapor water (kg/m^2/s^1)
J_w density of the mass flow of liquid water (kg/m^2/s^1)
K_H Henry's constant (-)
K_v intrinsic permeability (m^2)
Kw intrinsic permeability of the material (m^2)
K_{rv} gas relative permeability respectively
Krw relative permeability to liquid (-)
M_v molar mass of water vapor (kg/mol)
M_w molar mass of water (g/L)
n number of moles of Ca per mole of CSH (-)
$n_{Ca(OH)2}$ number of moles per volume of material for portlandite (mol/m^3)
n_{CSH} number of moles per volume of material for CSH (mol/m^3)
n_{CaCO_3} number of moles per volume of material for $CaCO_3$ (mol/m^3)
P_c capillary pressure (Pa)
P_v gas pressure in the pores (Pa)
Pvs saturated water vapor pressure (Pa)
Q_i heat released during hydration and the liquid-vapor phase change
R ideal gas constant (J/mol.K)
Ra air resistance (-)
T is the temperature (K)
$\bar{v}_{Ca(OH)_2}$ molar volume of portlandite
$\bar{v}_{CaCO_3}$ molar volume of $CaCO_3$ (m^3/mol)
W volume fraction of water (m^3/m^3)
$\Delta\bar{v}_{CSH}$ variation in volume associated with the carbonation of one mole of CSH (m^3/mol)
α molar fraction of $Ca(OH)_2$ carbonated
β_{H_2O} source term used to model the release of liquid water during carbonation of portlandite
$\delta^0_{Ca(OH)_2}$, consumption rates of portlandite (mol/m^3/s)
δ^0_{CSH} consumption rates of CSH (mol/m^3/s)
λ_{eff} effective conductivity of the medium under consideration (W/m.K).
λ^{ref}_{eff} effective thermal conductivity of the material at the reference condition (W/m/K)
μ_v represents the dynamic viscosity of the gas and gas pressure in the pores (Pa).
μ_w dynamic viscosity of liquid water (Pa.s)
ρ_c density of the cementitious material (kg/m³)
ρ_v density of liquid water vapor (kg/m^3)
ρ_w density of liquid water (kg/m^3)
τ_{CH} characteristic time of the chemical reaction of dissolution of $Ca(OH)_2$ (s)
τ_{CSH} characteristic time of the carbonation reaction of CSH (s)
φ porosity (-)
$[CO_2]$ concentration of CO_2 in the gaseous phase (mol/m^3)

1 Introduction

Nowadays, huge amounts of construction and demolition wastes are generated so that their management has become a serious social and environmental issue. Several regions also suffer from a serious shortage of natural aggregates for the production of new concretes [1]. In this context, the reuse of construction wastes is a very interesting strategy that allows to protect the natural mineral resources and landscapes but also to achieve sustainable development in the construction sector [2] [3].

Compared to typical natural aggregates (NA), recycled concrete aggregates (RCA) have a lower quality [1] [4] due to higher porosity. The concrete strength thus decreases when NA are totally or partially replaced by RCA [5]. In recent years, the adoption of accelerated carbonation, which is part of Carbon Capture and Utilization (CCU) methods [6] [7] has been proposed to improve RCA quality [8] [9] [10]. The treatment involves CO_2 reacting with the adhesive paste on RCA to produce calcium carbonate and silica gel. Key factors influencing this carbonation process in cement-based materials include temperature, relative humidity, and CO_2 availability. Thermo, hydro, and chemical processes intricately shape carbonation kinetics. Elevated temperatures accelerate diffusion and reaction rates, and influence reactants solubilities. Changes in relative humidity and moisture content impact CO_2 transport and reactants dissolution, facilitating or hindering carbonation reactions. Chemical reactions, such as calcium hydroxide dissolution and calcium carbonate precipitation, are thermodynamically influenced by temperature and moisture, further impacting reaction rates and product formation. The solid volume of the adhesive paste increases after carbonation, resulting in higher compressive strength, greater density, and lower absorption and porosity of RCA [11].

The carbonation of recycled concrete aggregates (RCA) not only enhances their own properties and those of concretes made from them but also enables the capture of carbon dioxide, thus mitigating the greenhouse effect [2] [12] [13]. Under atmospheric conditions, carbonation of concrete occurs, but the process is slow [14]. It is noteworthy that buildings contribute to approximately 30% of global carbon emission and cement industry is one of the main sources of greenhouse gases emissions, in particular carbon dioxide, which represent about 5 to 8% of total emissions [15]. The CO_2 concentration in cement plant fumes is about 15%, *i.e.* 360 times the atmospheric CO_2 concentration, and thus they offer a great potential to achieve accelerated carbonation of RCA as addressed in the National French Project FastCarb [10] [12]. During this project, the feasibility of CO_2 uptake by recycled concrete aggregates (RCA) in industrial conditions was demonstrated through the setup of two large-scale reactors utilizing cement

plant fumes. These demonstrators successfully carbonated several tons of RCA, achieving a maximum CO_2 fixation of 30 kg per ton of RCA in less than 1 hour, with the temperature maintained at approximately 80°C. To further optimize this industrial process and maximize its efficiency, a comprehensive understanding of high-temperature carbonation phenomena is essential. It is noteworthy that Artificial Intelligence (AI) has begun to be used to optimize and predict the carbonation of concrete [16] [17].

Research on the impact of temperature on the carbonation of cementitious materials under controlled conditions is limited in the literature, with less than twenty references (see below) in the past fifty years. Temperature plays a crucial role in water transfers and chemical reactions, influencing the physical properties of water, water vapor sorption isotherms, and material transport properties [16]. Higher temperatures are expected to promote water transport, affecting CO_2 penetration and water availability for carbonation reactions based on the material initial moisture state. Additionally, temperature significantly affects the kinetics and mechanisms of carbonation: while the solubility of hydrates and carbon dioxide decreases with temperature, the chemical reaction rate and diffusion of carbon dioxide and ions are thermoactivated [17] [18] [19]. Assessing the overall effect is challenging due to the simultaneous occurrence of multiple phenomena with potentially counterbalancing effects.

Existing studies in the literature on carbonation of cementitious materials show varying conclusions about the effect of temperature. Some studies examined moderate temperatures below 45°C (Mori et al [20], Yanagi and tomosawa [21], Papadakis et al [22] , and Villain et al [23], Dheilly and Todu [24]), with Dheilly and Todu [24] suggesting slower carbonation at higher temperatures due to retrograde solubility of hydrates, while others observed faster carbonation at higher temperatures. However, the explanations were limited to applying the Arrhenius law for thermo-activation effects, lacking a comprehensive understanding of the underlying physico-chemical mechanisms. Furthermore, temperature effects were often studied independently of relative humidity. For instance, Liu et al [25] found an optimum carbonation temperature of approximately 60°C for 100% relative humidity. Drouet [17] demonstrated that carbonation depth depend on temperatures and composition, and an increase in temperature between 20°C and 80°C accelerated carbonation kinetics [26] [27].

Current numerical models [28] [29] [30] used to simulate carbonation in cementitious materials often assume isothermal conditions at 20°C, which may not accurately represent real scenarios, especially in accelerated carbonation using cement plant fumes or other industrial gases. While

these models have offered valuable insights into carbonation processes, their applicability is limited in cases where temperature variations significantly affect the outcomes. Consequently, there is a growing need for advanced numerical models that consider temperature-dependent parameters and non-isothermal conditions.

This research aims to enhance the understanding of high-temperature effects (on carbonation processes and incorporate temperature dependence into the governing equations that describe carbonation. Specifically, the study is focused on modeling non-isothermal accelerated carbonation at 80°C for mortar made with Ordinary Portland Cement (OPC), as 80°C is the temperature of cement plant fumes that are intended to be used for accelerated carbonation of RCA. Through experiments in controlled humidity and temperature conditions, the influence of high temperature on the physico-chemical mechanisms of carbonation is explored, particularly by improving the description of temperature effects on heat transfer, moisture evolutions, and chemical kinetics. Based on new experimental results, the improvement of the model developed by Achour *et al* [30] involves integrating heat transfer mechanisms between the cementitious material and the environment, while considering the influence of temperature on mass transfers, diffusion of carbone dioxyde, dissolution, and carbonation of hydration products. The generated model allows describing the spatiotemporal evolution of parameters that cannot be experimentally monitored, such as temperature, water saturation, and carbon dioxide concentration, throughout the material undergoing carbonation. It also allows a direct comparison with several experimentally determinable measurements, such as the remaining amount of portlandite and precipitated calcium carbonate. Whereas experimental measurements provide a limited number of data, this model provides a continuous spatiotemporal evolution of these parameters.

2 Carbonation model integrating the effect of temperature

The basic model adopted in this work is related to the model of Achour et al [30]. The latter models simulates the coupled transport of chloride ions and carbon dioxide in unsaturated concrete. In the present work, improvements have been made in order to account for the effects of temperature. Heat transfer was added to the model since the previous version considers isothermal conditions. This integration allowed modelling the time-evolution of the temperature throughout the sample. From the obtained evolution, the effect of temperature on both the water transfer and the diffusion of gaseous CO_2 was taken into account. The temperature effect has also been considered and incorporated into the carbonation process of portlandite and CSH.

The model considers the coupling between reactive transfers of CO_2 and water. The two primary conservation equations (1 and 2) are related to the volume fraction of water W (m^3/m^3) and the concentration of gaseous CO_2 $[CO_2]$ in unsaturated conditions (mol/m^3). These equations are coupled with consumption rates of hydrates, CSH, and portlandite by CO_2 which are considered as sink terms in the balance equation of gaseous CO_2 concentration (equation 2), while the amount of liquid water released by the carbonation of portlandite is considered as source term in the mass balance equation of water as given in equation 1. In equation 3, the evolution of porosity (φ) during carbonation is described through the variation of volume induced by the consumption of both portlandite and CSH but also by the formation of calcium carbonates. Such description is required in the model regarding the evolution of transfer properties, such as water permeability and gaseous diffusion coefficients with that of porosity. Consumption rates of portlandite and CSH are given respectively in equations 4 et 5 and completed by the formation rate of calcium carbonates (equation 6).

$$\frac{\partial}{\partial t}\left((\varphi - W + W.K_H)[CO_2]\right) = -div(J_c) - \delta^0_{Ca(OH)_2} - \delta^0_{CSH} \quad (1)$$

$$\frac{\partial(\rho_w W)}{\partial t} + \frac{\partial(\rho_V W_V)}{\partial t} = -div(J_w + J_V) + \beta_{H_2O} \quad (2)$$

$$\Delta\varphi = \bar{v}_{Ca(OH)_2}\left(n^0_{Ca(OH)2} - n_{Ca(OH)2}\right) + \Delta\bar{v}_{CSH}\left(n^0_{CSH} - n_{CSH}\right) - \bar{v}_{CaCO_3}\left(n^0_{CaCO_3} - n_{CaCO_3}\right) \quad (3)$$

$$\frac{\partial n_{Ca(OH)2}}{\partial t} = \delta^0_{Ca(OH)_2} \quad (4)$$

$$\frac{\partial n_{CSH}}{\partial t} = \delta^0_{CSH} \quad (5)$$

$$\frac{\partial n_{CaCO_3}}{\partial t} = \delta^0_{Ca(OH)_2} + n \cdot \delta^0_{CSH} \quad (6)$$

Where: J_c is the molar flux of carbon dioxide ($kg/m^2/s^1$); J_V is the density of the mass flow of vapor water ($kg/m^2/s^1$); J_w is the density of the mass flow of liquid water ($kg/m^2/s^1$); K_H the Henry's constant (-); n the number of moles of Ca per mole of CSH (-); $n_{Ca(OH)2}$, n_{CSH}, and n_{CaCO_3} the number of moles per volume of material for portlandite, CSH, and $CaCO_3$, respectively (mol/m^3); $\bar{v}_{Ca(OH)_2}$ the molar volume of portlandite (m^3/mol); $\bar{v}_{CaCO_3}$ the molar volume of $CaCO_3$ (m^3/mol); $\Delta\bar{v}_{CSH}$ the variation in volume associated with the carbonation of one mole of CSH (m^3/mol); β_{H_2O} is a source term used to model the release of liquid water during carbonation of portlandite; $\delta^0_{Ca(OH)_2}$, and δ^0_{CSH} the respective consumption rates of portlandite and CSH ($mol/m^3/s$); ρ_w is the density of liquid water (kg/m^3); ρ_v is the density of

196 liquid water vapor (kg/m^3); $[CO_2]$ is the concentration of CO_2 in the gaseous phase (mol/m^3).
197 The subscript "0" refers to the initial values of the variables, that is, before carbonation.

198 In order to consider the effect of temperature on these mechanisms, the modifications presented
199 in the following paragraphs were made to the basic equations of the model summarized above.

200 2.1 Heat transfer equation

201 Different modeling approaches are suggested in the literature to predict temperature fields in
202 porous materials. The most commonly used approach considers a single mass conservation
203 equation with average material parameters to account for the different phases [31]. Most of
204 existing studies are focused on the energy balance for each phase in the medium [31] [32].
205 Within an unsaturated medium, heat is actually transferred in three forms: conduction
206 respecting Fourier's law, convection due to the movement of liquid water and gases (water
207 vapor + dry air) and energy exchange (condensation or evaporation) between water and water
208 vapor [33]. The movement of the fluid in a cementitious material with fine porosity is very
209 slow, its contribution to the heat flow can therefore be considered as negligible compared to the
210 heat conduction. The heat flow (J_t) and the heat balance are expressed as follows:

$$J_t = \underbrace{-\lambda_{eff}\mathrm{grad}T}_{\text{Conduction}} + \underbrace{\left(C_{pv}\,\rho_v\,\frac{K_v K_{rv}}{\mu_v}\,\mathrm{grad}P_v\right)}_{\text{Internal energy of the gas}} T \qquad (7)$$

$$\rho_c C_P \frac{\partial T}{\partial t} + div(J_t) + \sum Q_i = 0 \qquad (8)$$

211 C_P is the heat capacity of the cementitious material (J.kg^{-1}.K^{-1}), C_{pv} denotes the thermal
212 capacity of the gas mixture (J.kg^{-1}.K^{-1}), K_v and K_{rv}, represent the intrinsic permeability (m^2)
213 and gas relative permeability respectively. P_v represents the gas pressure in the pores (Pa) and
214 T is temperature (K). The effective conductivity of the medium under consideration is
215 represented by λ_{eff}(W/m.K). μ_v represents the dynamic viscosity of the gas. ρ_c is the density of
216 the cementitious material (kg/m³).

217 Q_i represents the heat released during hydration and the liquid-vapor phase change. However,
218 the heat release caused by the hydration of the cementitious material is only significant in the
219 first few hours [31]. Therefore, for a cementitious material studied over the long term, this term
220 is negligible.

221 The energy associated with the liquid-vapor phase change, as well as the heat carried by the gas
222 flow, have a negligible impact on the overall temperature field. This assumption was originally

proposed by Samson et al. [31] for temperatures up to 50°C. Given the scarcity of data for higher temperatures, this assumption will be upheld in our current study. Consequently, the heat balance can be expressed as:

$$\rho_c C_P \frac{\partial T}{\partial t} + div\left(\lambda_{eff} gradT\right) = 0 \quad (9)$$

In the existing literature, several experimental studies are aimed at determining the effective thermal conductivity (λ_{eff}) of materials. In this work, empirical laws have been chosen; they are also cited in references [33] and [31]. Specifically, when the temperature closely approximates the reference temperature of 293 K, the law can be represented as equation (10).

$$\lambda_{eff} = \lambda_{eff}^{ref}(0.244(\frac{W}{\varphi} + 0.756)) \quad (10)$$

Where λ_{eff}^{ref} the effective thermal conductivity of the material measured at the reference condition (W/m/K).

Solving equation (9) requires the knowledge of water content involved in conductivity ((10). This parameter reflects the coupling between moisture transfer and heat transfer.

2.2 Water transport

Considering the convective movement of water and the diffusive movement of water vapor and applying the mass conservation law, the transfer of water in a cementitious material is described by equation (2) [30]. The effect of temperature is taken into account in both liquid water transport and vapor transport, as described in the following sections.

It is noteworthy that the assumptions made include the pressure of the gas mixture remaining constant during the transfer mechanisms of carbon dioxide, and that the density of dry air is negligible compared to that of liquid water.

2.2.1 Transport of liquid water

The convective transport of liquid water is driven by a water pressure gradient under isothermal conditions. Given that variations of temperature are considered in the model, the density of the mass flow of liquid water J_w (kg.m^{-2}. s^{-1}), described by equation (11), also includes a term related to the temperature gradient

$$J_w = \rho_w \frac{K_w K_{rw}}{\mu_w}\left(\frac{\partial P_C}{\partial W} grad(W) + \frac{\partial P_C}{\partial T} grad(T)\right) \quad (11)$$

Where:

- K_{rw} (-): relative permeability to liquid, considering the connectivity of the liquid phase when the material is partially saturated.
- K_w (m^2): intrinsic permeability of the material.
- P_C (Pa): capillary pressure, defined by Laplace's law as the difference between the pressure of gas (P_g) and that of water (P_w). Given that P_g is assumed to be constant and negligible compared to P_w, P_w can be directly related to P_C which can be expressed as function of other variables such as temperature and water content. This is the reason why capillary pressure is involved in equation 11 instead of water pressure.
- μ_w (Pa.s): dynamic viscosity of liquid water. Viscosity decreases as temperature increases. This decrease in water viscosity promotes liquid permeation at high relative humidity during drying processes, as well as increased gas-phase transportation due to more significant evaporation and thermal agitation of gas molecules.

2.2.2 Transport of water vapor

The gas phase is considered to be an ideal gas comprising inert dry air and water vapor. The transfer of water vapor in dry air is governed by diffusion according to Fick's law. Due to variations of temperature considered in the model, we have to take into account the temperature gradient in addition to water content gradient in the present study.

$$J_V = -R_a D_{va}\left(\frac{M_V}{RT}P_{VS}\frac{\partial\left(e^{-\frac{P_C M_v}{\rho_w RT}}\right)}{\partial W}grad(W) - \frac{M_V}{R}e^{-\frac{P_C M_v}{\rho_w RT}}\frac{\partial\left(\frac{P_{VS}}{T}\right)}{\partial T}grad(T)\right) \quad (12)$$

Where

- D_{va} (m^2/s): diffusion coefficient of water vapor in the air
- M_v (kg/mol): molar mass of water vapor
- P_{vs} (Pa): saturated water vapor pressure
- R (J/mol.K): ideal gas constant
- R_a (-): air resistance related to the characteristics of the porous network, including the effects of tortuosity and the degree of saturation. Millington's empirical expression is used to account for the reduction factor in water vapor transfer expressed in the following equation:

$$Ra = \varphi^{2.74}\left(1 - \frac{W}{\varphi}\right)^{4.2} \quad (13)$$

2.2.3 Conservation equation of water

From equations (11) and (12), equation (2) can be rewritten as follows:

$$\frac{\partial(\rho_w W)}{\partial t} + div(\rho_w \frac{K_w K_{rw}}{\mu_w}\frac{\partial P_C}{\partial W} grad(W) + \rho_w \frac{K_w K_{rw}}{\mu_w}\frac{\partial P_C}{\partial T} grad(T) + R_a D_{va}\frac{M_V}{RT} P_{VS}\frac{\partial\left(e^{\frac{-P_C M_v}{\rho_w RT}}\right)}{\partial W} grad(W) + R_a D_{va}\frac{M_V}{R} e^{\frac{-P_C M_v}{\rho_w RT}}\frac{\partial\left(\frac{P_{VS}}{T}\right)}{\partial T} grad(T)) + \frac{\partial[Ca(OH)_2]M_w}{\partial T\ \rho_e} = 0 \quad (14)$$

276 M_w (g/L) represents the molar mass of water

277 The two parameters $\rho_w \frac{K_w * K_{rw}}{\mu_w}\frac{\partial P_C}{\partial T}$ and $R_a D_{va}\frac{M_V}{R} e^{\frac{-P_C M_v}{\rho_w RT}}\frac{\partial\left(\frac{P_{VS}}{T}\right)}{\partial T}$ related to the temperature
278 gradient represent the permeation of liquid water and the diffusion of water vapor generated by
279 a temperature gradient, respectively.

280 2.3 Physical and chemical mechanism of carbonation

281 2.3.1 Diffusion and dissolution of gaseous carbon dioxide

282 According to the perfect gas law P.V= n.R.T, at constant pressure, the concentration of the gas
283 (n/V) decreases with increasing temperature. Therefore, during accelerated carbonation, if the
284 percentage of carbon dioxide is maintained at 15%, its concentration decreases with increasing
285 temperature.

286 The transfer of carbon dioxide is considered diffusive through the gas phase. The expression
287 for the molar flux of carbon dioxide under isothermal conditions is given by equation (15)
288 assuming that the total gas pressure is constant and equal to atmospheric pressure [29].

$$J_c = -D_{CO_2}(\varphi, W)\ grad[CO_2] \quad (15)$$

289 D_{CO2} (m^2/s) : coefficient of diffusion for gaseous CO_2

290 Thiery [28] calibrated the Millington expression for calculating the diffusion coefficient of
291 carbon dioxide, considering the tortuosity of pore network and saturation level. This calibration
292 involved comparing numerical results with experimental tests [34], leading to equation (16).

$$D_{CO_2} = D^0_{CO_2} * \varphi^{2.74}(1 - \frac{W}{\varphi})^{4.2} \quad (16)$$

293 $D^0_{CO_2}(m^2/s)$: Diffusion coefficient of carbon dioxide in the air at 25°C

The increase in temperature leads to an acceleration of CO_2 diffusion in the cementitious matrix [17]. Some authors [17] [35] have used the well-known Arrhenius law (17) to account for the temperature dependence of the CO_2 diffusion coefficient in cementitious material.

$$D = D^0 e^{\frac{-E_a}{R T}} \quad (17)$$

E_a: (J/mol) : activation energy

As first step, this law was used. The activation energy E_a is about 15 to 20 kJ/mol [36] [37] for the gaseous diffusion of CO_2. In this study, the value of E_a was 15 kJ/mol.

It is noteworthy that the diffusion of CO_2 through the concrete matrix can be significantly influenced by factors like cracking, which might not be fully accounted for in the model (for example, in the equation of the CO_2 diffusion coefficient). Nonetheless, cracking is considered in the parameters derived from experimental results, such as the sorption-desorption isotherm.

CO_2 dissolves in the pore solution depending on the water saturation state of the cementitious material. Its dissolution depends on the partial pressure of CO_2 in the air, the temperature and the presence of other ions in the solution [15]. Gilbert *et al.* [15] showed that the solubility of CO_2 decreases with increasing temperature and ionic strength. Once dissolved in solution, a small amount hydrolyzes to form carbonic acid (H_2CO_3), which dissociates to form bicarbonate (HCO_3^-) and carbonate (CO_3^{2-}). The concentration of the acid is given by Henry's law as a function of the concentration of CO_2 in the gas phase:

$$[H_2CO_3] = K_H\,[CO_2] \quad (18)$$

Henry's "constant" K_H is not a true constant, but instead it has a significant nonlinear dependence on temperature [38]. In order to predict the value of this constant at a given temperature T, an extrapolation method using the enthalpy of the solute of the solution ΔH_{sol} by means of a thermodynamic expression, usually associated with the name van't Hoff can be used [39].

$$\frac{K_H(T_i)}{K_H(T_0)} = \frac{T_i}{T_0}\, e^{\left[\left(\frac{\Delta H_{sol}}{R}\right)\left(\frac{1}{T_i}-\frac{1}{T_0}\right)\right]} \quad (19)$$

2.3.2 Kinetics of carbonation of portlandite $Ca(OH)_2$ and calcium silicate hydrates CSH

In this model, the carbonation of portlandite and calcium silicate hydrates (CSH) is assumed to predominate, while the carbonation of other hydrates is neglected. This simplification is

justified due to the significant reactivity and quantity of portlandite and CSH in the cement matrix. By assimilating the crystalline clusters of portlandite to monodisperse spheres, Thiery et al [40] demonstrated that the dissolution kinetics of portlandite hampered by $CaCO_3$ precipitation can be written as follows:

$$\delta^0_{Ca(OH)_2} = \frac{W}{\tau_{Ca(OH)_2}} n^0_{Ca(OH)_2} V_{Ca(OH)_2} K_H \frac{(1-\alpha)}{[1-(1-\alpha)^{\frac{1}{3}}]} [CO_2] \quad \textbf{(20)}$$

τ_{CH} (s) : characteristic time of the chemical reaction of dissolution of $Ca(OH)_2$

α is the molar fraction of $Ca(OH)_2$ carbonated expressed as follows:

$$\alpha = 1 - \frac{n_{Ca(OH)_2}}{n^0_{Ca(OH)_2}} \quad \textbf{(21)}$$

The carbonation kinetics of hydrated calcium silicates (CSH) is assumed to be first order with respect to the CO_2 concentration in the gas phase [40]. Thus, the consumption rate of CSH (δ^0_{CSH}) is calculated by equation (22):

$$\delta^0_{CSH} = W \frac{K_H}{\tau_{CSH}} [CO_2] \quad \textbf{(22)}$$

τ_{CSH} (s) : characteristic time of the carbonation reaction of CSH.

In case of non-isothermal carbonation in an environment with a temperature above 20°C, the effect of temperature is taken into account in the following parameters: water content W, carbon dioxide concentration $[CO_2]$, Henry's constant K_H, characteristic time of carbonation of portlandite τ_{CH} as well as the characteristic time of carbonation of calcium silicate hydrate τ_{CSH}. Both portlandite and CSH exhibit retrograde solubility with temperature [41]. The parameters τ_{CH} and τ_{CSH} are therefore temperature dependent. To the best of our knowledge, no studies have been proposed in the literature about the effect of temperature on these parameters. Thus, in the present study, the calibration of these parameters were performed at 20 and 80°C based on the experimental results. The tests at 20°C were performed in order to validate the calibration method used by comparing the results obtained in this study with those already available in the literature.

2.4 Numerical resolution

The numerical simulation is conducted using MATLAB, wherein the equations are numerically resolved on a one-dimensional (1D) geometry. The study focuses on a mortar specimen of length H, which is exposed to an atmosphere with given concentration of CO_2 and relative

humidity at x = 0. The specimen is sealed on all sides, except for the transverse side at x = 0, to achieve a unidirectional carbonation process. Several numerical methods can be considered for this scenario. However, for this particular set of non-linear equations, the most suitable method is the finite volume method. It is widely used for solving transfer problems associated with physico-chemical reactions [28].

The adopted numerical scheme is the implicit Euler scheme for water and heat transfer. This scheme is chosen due to its unconditional stability [30] [33]. However, for the carbon dioxide transfer, the explicit Euler scheme is used, which requires stability verification at each iteration [30] [33].

As for the boundary conditions, the Dirichlet condition is applied to the water transfer and carbon dioxide transfer problems, while the Newton Fourier condition is employed for heat transfer. The studied transfer phenomena are unidirectional, and the spatial mesh used is described in figure 1.

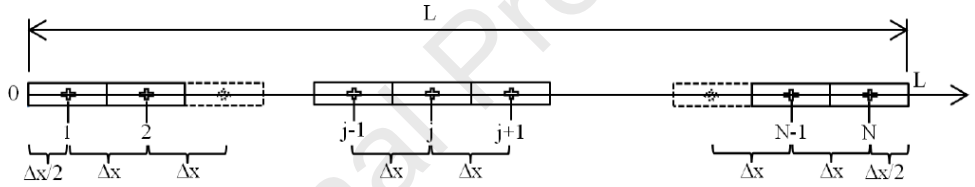

Figure 1: Mesh adapted for numerical resolution [33]

The input data of the model are the environmental conditions: temperature, relative humidity and CO_2 concentration, as well as the properties of the material before carbonation: porosity, intrinsic permeability, water content (or saturation degree), sorption-desorption isotherm curves and the initial quantities of portlandite and CSH. As outputs, the model is able to provide the evolution of the portlandite and CSH contents as well as different profiles on carbonated materials such as those of calcium carbonates precipitation, silica gel, porosity, temperature and water content of the carbonated cementitious material at 20°C or 80°C under isothermal or non-isothermal conditions. Figure 2 describes the adopted modeling methodology. Table1 summarizes the expected effects of temperature on the main terms integrating temperature in the new version of the model proposed by Achour et al. [30]. Some effects are evaluated or calibrated from experimental results presented in section 4.

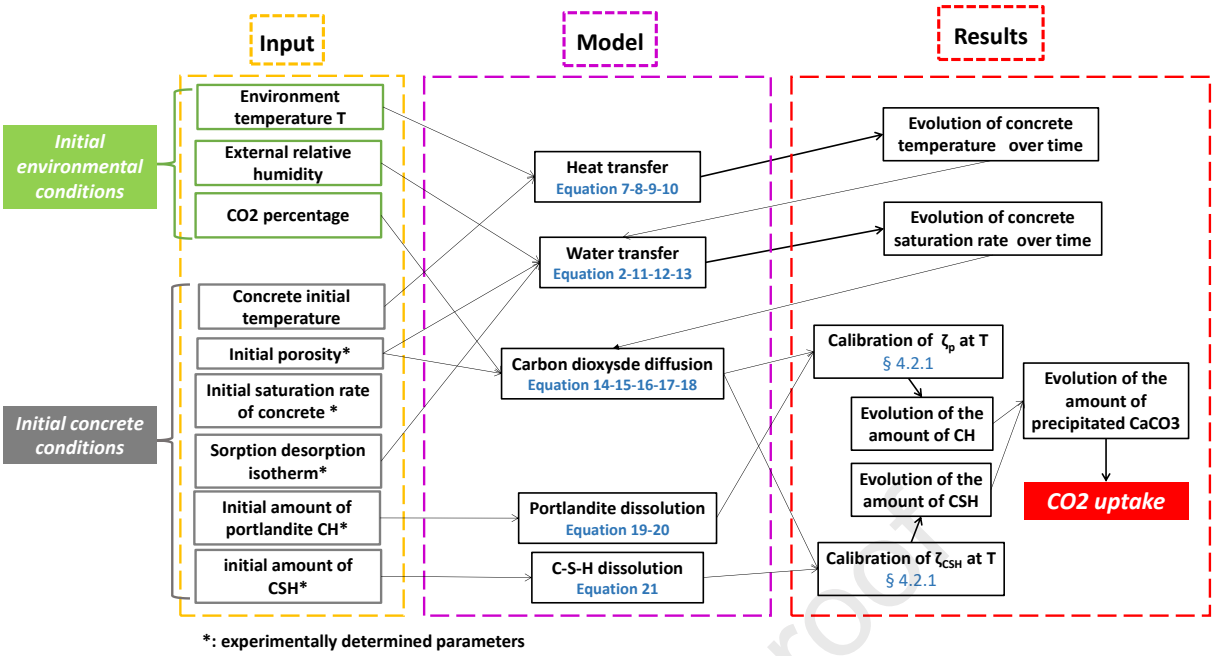

371

372 **Figure 2: Diagram of the modeling procedure**

373 **Table1: Summary of the impact of temperature on the transport systems in the model**
374

Transport system and main equations	Main parameters influenced by temperature	Comments
Water transport equation (14)	Parameters $\boldsymbol{\rho_w} \frac{K_w * K_{rw}}{\mu_w} \frac{\partial P_C}{\partial T}$ and $\boldsymbol{R_a D_{va}} \frac{M_V}{R} \boldsymbol{e}^{\frac{-P_C M_v}{\rho_w RT}} \frac{\partial\left(\frac{P_{VS}}{T}\right)}{\partial T}$ related to the temperature gradient	See section 4.1.3
	Viscosity μ_w	Increasing temperature leads to a decrease in viscosity, resulting in faster heat transfer.
	Sorption –desorption isotherme $(\frac{\partial P_C}{\partial W})$	See section 4.1.3
	Term RT	Increase in temperature results in faster transfer.
Diffusion and dissolution of CO_2	Coefficient of diffusion for gaseous CO_2 $\mathbf{D_{CO2}}$	Increase with temperature. Arrhenius law

equations (15)		$\frac{\mathbf{D_{CO2}}\ \boldsymbol{at\ 80°C}}{\mathbf{D_{CO2}}\ \boldsymbol{at\ 20°C}} = \mathbf{2.84}$ Faster diffusion at higher temperatures.
	Henry's constant K_H	Decrease with temperature. van't Hoff extrapolation $\frac{\boldsymbol{K_H\ at\ 80°C}}{\boldsymbol{K_H\ at\ 20°C}} = \mathbf{0.299}$ lower dissolution of CO_2 at higher temperatures
Carbonation of $Ca(OH)_2$ and CSH **equations (20) and (22)**	$\boldsymbol{\tau_{CH}}$ and $\boldsymbol{\tau_{CSH}}$	See section 4.2.1

3 Experimental study

3.1 Materials and samples preparation

The cement used for the preparation of the mortar used in this study was an ordinary Portland cement CEM I 52.5 from Villiers-au-Bouin, France. The cement composition is given in Table 2. Its absolute density was 3.13 g/cm^3 and its specific surface area was 3,900 cm^2/g.

Table 2: Chemical composition of the used cement

Oxide constituents (%)									
CaO	SiO_2	Al_2O_3	MgO	Fe_2O_3	SO_3	TiO_2	K_2O	Na_2O	P_2O_3
63.70	19.60	4.50	3.90	2.30	2.60	0.20	0.70	0.13	0.20

Natural siliceous sand (0-2 mm) had a specific density of 2.61 g/cm^3. A purely siliceous sand was chosen to be sure that the observed calcium carbonate only originates from the carbonation of the cement paste. Cement mortar was prepared with the following mass proportions (cement; sand; water): 1; 2.6; 0.6. A high w/c ratio accelerates the diffusion of carbon dioxide and therefore the carbonation during the experimental study.

Cylindrical samples were cast in molds of Ø 110 × 220 mm (cardboard molds covered with plastic). The samples were demolded after 24 h and then stored in a tap water tank for 180 days at 23 ± 1°C (Figure 3). The purpose of this long curing time is to achieve a high degree of hydration, so that the mortar is more representative of an old mortar in RCA. After curing, a preconditioning was carried out before accelerated carbonation tests. The samples were dried at 40°C for 10 days, and then stored for 1 year in an air-conditioned room (T = 20°C, RH = 55 %) to homogenize the internal humidity. A temperature of 40°C was chosen to dry the material without affecting the structure of hydration products. The purpose of such preconditioning was to reach a hydric state of samples close to the equilibrium with the relative humidity of the environment chosen for the carbonation stage (i.e., 65% RH). Additionally, it allows aging the mortar and ensures an initial natural carbonation so that it is more representative of the mortar in RCA.

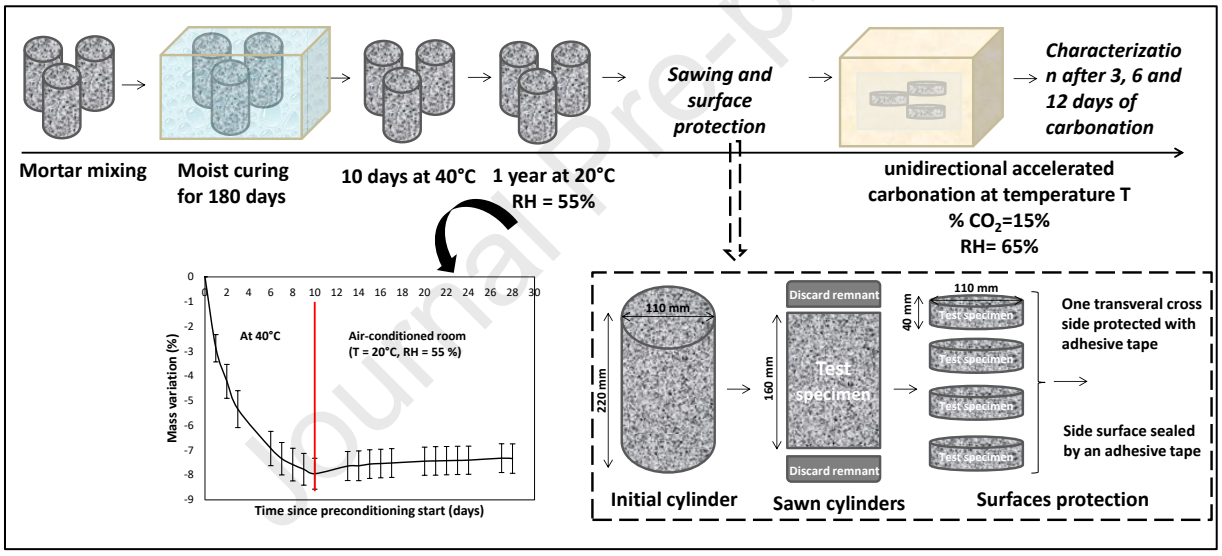

Figure 3: Schematic representation of experimental procedure

3.2 Accelerated carbonation procedure (treatment)

Prior to carbonation, each 220 mm cylinder was sawn transversely into four 40 mm high cylinders (Figure 3). These specimens were then protected by an adhesive aluminum on their side surface and one transversal cross section of the sawn surfaces in order to ensure an unidirectional diffusion of CO_2. Then, the four specimens of the same cylinder were subjected to unidirectional carbonation in a climate chamber at 65% RH and 15% CO_2 at a given temperature. Two temperatures were tested: 20°C and 80°C. The temperature, relative humidity and CO_2 concentration in the chamber were automatically controlled at 80°C and 15% CO_2, which are the typical temperature and CO_2 content of cement plant fumes respectively. Figure

3 describes the experimental program. At the beginning of the carbonation stage, the temperature of specimens was 20°C. Therefore, in the case of carbonation at 80°C, the specimens were brought to thermal and hydric equilibrium from 20°C and 55% RH to 80°C and 65% RH.

For each of the two temperatures, an initial characterization was carried out before carbonation, followed by characterizations after 3, 6, and 12 days of carbonation. The materials characterization includes the evolution of the composition (TGA and XRD), water-accessible porosity, carbonation depth, and sorption-desorption isotherms.

The experimental study (accelerated carbonation) was carried out according to the parameters of gaz (T and HR) of the cement industry tested in the National Project FASTARB [8], the optimum relative humidity being between 50 and 80% and temperature between 70°C and 90°C.

This research can be used to choose the pre-treatment of recycled concrete aggregates before accelerated carbonation. For instance, it has been experimentally shown that an initial water saturation of 80% was optimal in terms of bound CO_2 content for a given carbonation time.

3.3 Material characterization

3.3.1 Thermogravimetric analysis (TGA)

The thermogravimetric analysis was performed using a NETZSCH microbalance. The carbonation was unidirectional and the external carbon dioxide diffused from only one side of the sample, as shown in Figure 3. In order to evaluate the evolution of the mineralogy and the progression of the carbonation with depth, TGA tests were performed on samples taken at three different depths after different carbonation durations as indicated in Figure 4. The sample taken at depth 1 is in direct contact with carbon dioxide. The second and third samples, taken at depths 2 and 3, respectively, are increasingly distant from the specimen surface. To prepare the TGA sample, the piece of mortar was manually ground and sieved to 80 μm. Intensive, manual grinding was performed in an attempt to get all the cement paste in the test sample through the sieve. The resulting powder sample, with a mass around 120 mg, was collected in an alumina crucible and placed in the thermal balance. The tests were performed under a nitrogen stream in the temperature range from 20°C to 1000°C with a heating rate of 10°C per minute.

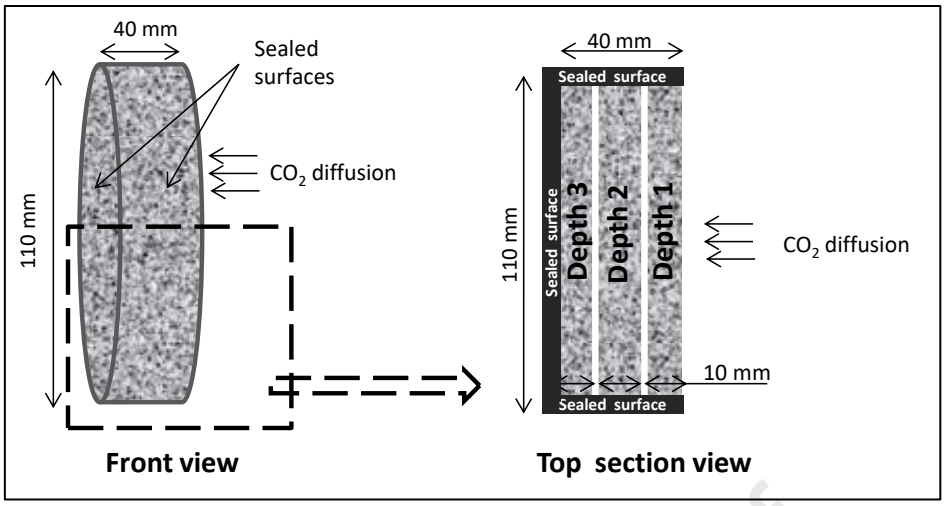

Figure 4: Schematic drawing of ATG sampling

Many authors have identified the decomposition temperature ranges of the phases of cement-based materials [17] [42]. These temperatures are likely to vary as a function of measurement parameters (heating rate, number of measuring heads and type of sample holder) or sample properties (density, mass, carbonation) [43] [44] [45]. In this study, the limit temperatures are defined by the edges of the characteristic peaks of the DTG curve [46] [28] [45].

3.3.2 X-Ray diffraction (XRD)

XRD analyses were carried out on a Malvern Panalytical Aeris instrument. It combines two technologies from Aeris and Zetium and provides full material characterization by adding information about elemental composition determined by Zetium to the phase identification from Aeris. Scanning program consisted in rotating between 7 and 70°2θ with a step size of 0.01°2θ and a time per step of 480.165 ms. XRD analyses were performed on samples prepared as for TGA, taken at the three different depths (Figure 4) and at different carbonation times.

3.3.3 Dynamic Vapor Sorption (DVS)

Dynamic Vapor Sorption (DVS) is a gravimetric sorption technique that allows determining the rate and amount of solvent absorbed by a sample. The sample is placed in a humidity and temperature controlled chamber. This technique automatically generates different humidity levels to determine the vapor water sorption/desorption isotherm. Accurate monitoring of the mass at regular time intervals is performed. To determine when equilibrium is reached, the instrument records the rate of mass variation (dm/dt). The criterion used to generate the next moisture content is a critical time defined prior to the test and selected based on the sample being tested.

In this study, the determination of vapor water sorption-desorption isotherm was performed using Hiden Isochema /unIgASorb CT. It is a fully automated dynamic vapor sorption analyzer operating at temperatures from 5 to 85°C and moisture contents from 0 to 98%. Non-carbonated samples and samples carbonated at 20°C and carbonated at 80°C were ground then tested. Two external temperatures were tested: 20°C and 80°C. Table 3 gives the parameters of the tests.

Table 3: DVS test conditions and carbonation parameters of tested samples

	DVS temperature: 20°C	**DVS temperature: 80°C**
Non carbonated sample	Sample 1	Sample 4
Sample carbonated at 20°C	Sample 2	Sample 5
Sample carbonated at 80°C	Sample 3	Sample 6

4 Results and discussion

4.1 Experimental results

4.1.1 Carbonation depth

The depth of carbonation was measured using a phenolphthalein spray. Phenolphthalein, a common pH indicator, changes color as carbonation advances. Initially pink (basic medium), it turns colorless as the alkaline concrete reacts with CO_2 to form carbonate ions. This color change allows to assess the displacement of the carbonation front over time. The value displayed in Figure 5 represents the average of ten measurements taken from two samples at each time. It is noteworthy to mention that the initial natural carbonation (in radial direction) was minimal and did not exceed 3 mm. This was confirmed through phenolphthalein testing and thermogravimetric analysis (ATG). The time-evolution of the carbonation depth was a linear function with the square root of the carbonation time for both temperatures (20°C et 80°C) [47]. The carbonation rate is assumed to account for both the composition of the cementitious material and the environmental conditions. The carbonation rate was higher at 80°C than at 20°C (0.39 vs. 0.24). Thus, the progression of carbonation front was accelerated by the increase in temperature.

Two phenomena with opposing effects can occur simultaneously with increasing temperature. Some researchers suggest that higher temperatures reduce carbonation due to lower dissolution of carbon dioxide in liquid water, evaporation leading to a lack of liquid water [19], and retrograde solubility of portlandite and CSH [48]. However, other authors argue that

temperature increase accelerates reaction kinetics [49] and the diffusivity of carbon dioxide and ions in cementitious materials, promoting carbonation [17], [50], [51]. Thermal expansion also reduces the resistance of porous medium to diffusion. Based on the results shown in Figure 5, increasing temperature accelerated carbonation in the temperature range of 20°C to 80°C at 65% relative humidity. It is noteworthy that carbonation depth indicated in Figure 5 was obtained from pH indicator, thus the corresponding data only provide indirect information on the carbonation process.

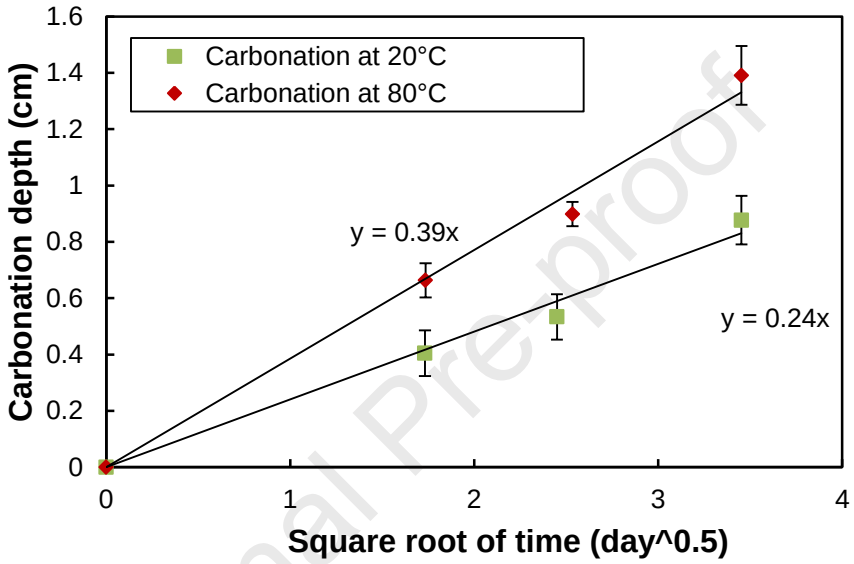

Figure 5: Evolution of carbonation depth during carbonation at 20°C and 80°C

The unidirectional carbonation of mortar samples was monitored for 12 days. During these 12 days, carbonation did not reach the samples taken at depths 2 and 3 (the maximum depth of carbonates was 1.4 cm). Therefore, for the following tests (ATG, DRX and DVS), the evolution in time of the sample taken at depth 1 is studied.

4.1.2 Mineralogical changes

Figure 6 and Figure 7 respectively show the results of DTG and XRD analyses performed on mortar samples taken at depth 1 and carbonated for 12 days at two different carbonation temperatures (20°C and 80°C) and at the same relative humidity (65%).

TGA and XRD are highly effective techniques for identifying calcium carbonate polymorphs and other crystalline phases formed during carbonation. TGA quantifies carbonate formation by analyzing weight loss during controlled heating, providing quantitative data on carbonation depth. XRD identifies crystalline phases, including calcium carbonate, enabling visualization

of the carbonation front over time. These methods offer both qualitative and quantitative information about material composition and carbonation progression. The combination of all these methods provides a comprehensive understanding of carbonation evolution and carbonation depth. Figure 8 illustrates the evolution of the CO_2 uptake quantity calculated from the DTG results.

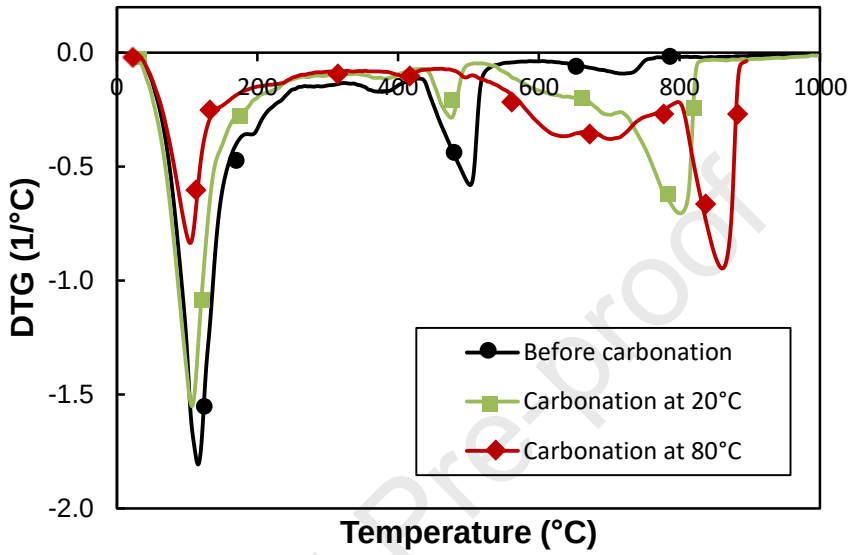

Figure 6: DTG curves of samples taken at depth 1 carbonated for 12 days at 20°C and 80°C

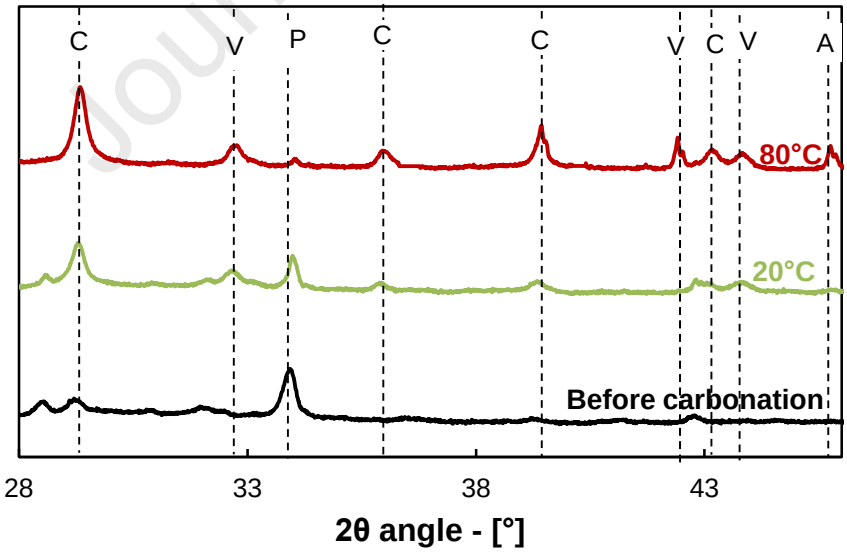

Figure 7: XRD curves of samples taken at depth 1 carbonated for 12 days at 20°C and 80°C. The different phases are labeled on the graph, with "P" indicating portlandite and the calcium carbonate polymorphs identified as "V" for vaterite, "A" for aragonite, and "C" for calcite

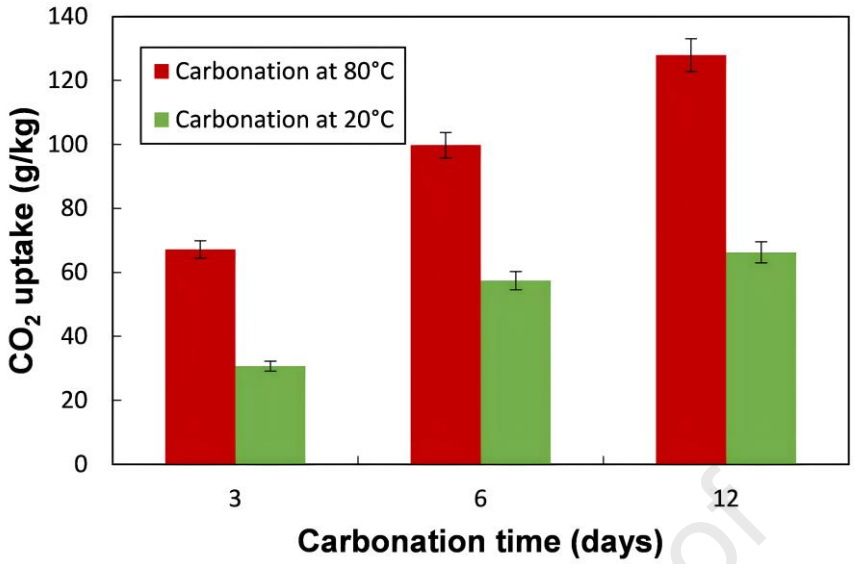

520

521 **Figure 8: CO_2 uptake during carbonation at 20°C and 80°C of samples taken at depth 1.**
522 **Calculations were performed based on the dry mass of the sample at 950°C**

523 For samples carbonated at 20°C, the portlandite peak between 400°C and 600°C can still be
524 distinguished after 12 days of carbonation whereas this peak is no longer visible after 12 days
525 of carbonation at 80°C. These results are in agreement with the results of the XRD analysis.
526 The peaks of the formed calcium carbonate polymorphs appearing between 600°C and 850°C
527 on XRD and DTG curves are more pronounced for carbonation at 80°C than for carbonation at
528 20°C. This result is also confirmed by the higher quantity of CO_2 uptake observed at 80°C
529 during carbonation. Thus, in addition to the carbonation depth results presented in the previous
530 section, the DTG and XRD results also confirm that the carbonation kinetics, in terms of
531 carbonation front and reactions, is accelerated by the temperature increase from 20°C to 80°C.
532 The effect of thermo-activated transport dominated the retrograde solubility of the reactants.

533 XRD results are analyzed to evaluate qualitatively the polymorphic abundance of calcium
534 carbonate (calcite, aragonite and vaterite [52]) in the carbonated zone . Regardless of
535 temperature, the XRD results show precipitation of the three usual polymorphs of calcium
536 carbonate. It is noteworthy that the vaterite and aragonite peaks are small in the carbonated
537 sample at 20°C, where portlandite is still present, while they are significantly higher in the
538 carbonated sample at 80°C, where portlandite is depleted. These observations confirm that
539 portlandite is carbonated from the first stages of carbonation. In a basic medium, this leads to
540 the precipitation of calcite [53] [54], which is the stable polymorph of calcium carbonate. As
541 carbonation progresses, portlandite is depleted and the pH of the concrete decreases. CSH
542 carbonation begins to predominate [27], leading to the precipitation of unstable polymorphs of

543 $CaCO_3$ (aragonite and vaterite) [17] [55]. The carbonation of aluminates was not taken into
544 account in this study. The XRD results at 80°C show a disappearance of the ettringite peak,
545 which is consistent with the well-known decomposition of ettringite at this temperature.

546 ### 4.1.3 Sorption - desorption isotherms

547 Figure 9 and Figure 10 show the sorption-desorption isotherms obtained using the sorption
548 balance (DVS) at 20°C and 80°C respectively. For each temperature, sorption-desorption
549 isotherms were measured on three samples taken from the first 10 cm (depth 1).

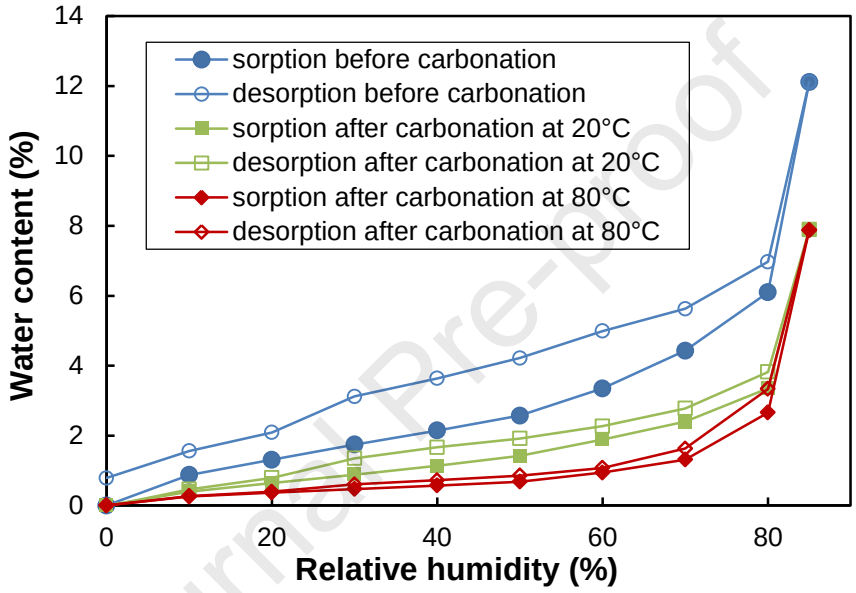

550

551 **Figure 9: Sorption desorption isotherms at 20°C, samples taken at depth 1**

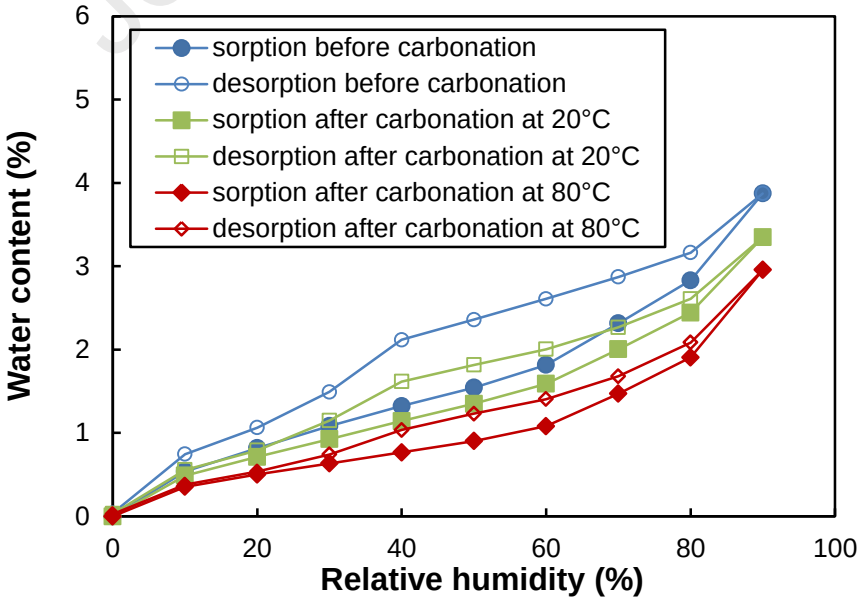

552

553 **Figure 10: Sorption desorption isotherm at 80°C, samples taken at depth 1**

For both temperatures test (20°C and 80°C), carbonation resulted in a significant decrease in equilibrium water content. This decrease in water retention capacity is directly linked to the clogging of the pores and the modifications of the porous structure [56] by the calcium carbonate crystals produced during carbonation. This clogging of the pores as a result of carbonation leads to homogenization of the internal radius of the pores and probably reduces the ink bottle effects resulting in the observed reduction of the isotherm hysteresis [57]. As mentioned before, experimental results (TGA, XRD and carbonation depth) confirm that the carbonation kinetics are accelerated by the temperature increase from 20°C to 80°C. This explains the most significant decrease in the saturation rate observed after carbonation at 80°C compared to 20°C.

By comparing Figure 9 to Figure 10, it is clear that the temperature of the external environment of the mortar had a considerable impact on the sorption-desorption isotherm. For a given RH, the equilibrium water content was systematically lower at 80 °C (Figure 9) compared to the tests performed at 20 °C (Figure 10). Such trends have already been observed by other researchers who have worked on the influence of temperature on water equilibria and transfers [17] [51] [58]. The decrease in water content at saturation can be explained by the decrease in water density with increasing temperature [59]. In addition to the fact that temperature affects the physical properties of water such as its density and viscosity, the radius of pores (Rp) emptied or filled with water at a given relative humidity also decreases with temperature as predicted by the Kelvin-Laplace relationship equation ((23).

$$Rp = \frac{2\sigma Mv}{\rho_l \, RT \, ln(h)} \qquad \textbf{(23)}$$

Where: h is the relative humidity (-), Mv the molar mass of water vapor (kg/mol), ρ_l the density of water (kg/m^3) and σ the water-vapor interfacial tension (N/m).

It should be noted that an increase in intrinsic permeability linked to an increase in temperature could be a consequence of a widening of the microcracks [60] and an increase in porosity [59]. In addition to the reasons already mentioned, the reduction of the water content at equilibrium can be explained by the principle of Le Chatelier [59]. The latter stipulates that a tendency to modify the conditions of a system in equilibrium results in a partial opposition to the changes imposed on it until a new state of equilibrium is established. Elevating the temperature initiates an equilibrium shift, leading to a subsequent decrease in temperature, which in other words implies heat absorption. Adsorption is an exothermic process [59] while desorption is an

endothermic process. Thus, according to Le Chatelier's principle, increasing temperature hinders adsorption and favors desorption, resulting in fewer molecules that can be adsorbed during adsorption and more that can be desorbed during desorption. The reduction in equilibrium water content was not constant over the entire RH range; for example, at 80% RH, the difference in water content for a non-carbonated sample was about 3.26% (absolute value), whereas it was about 0.66% at 30% RH.

The value of $\frac{\partial P_C}{\partial W}$ used in the model, derived from isotherm curves, is temperature-dependent but it does not fluctuate with changes in temperature. For example, when a sample at 20°C is transferred into an environment at 80°C, the 80°C isotherm can be used because heat transfer is relatively fast in cementitious material [61] [62]. Figure 11 illustrates the temperature evolution of the 40 mm mortar sample placed at 80°C. The results demonstrate that it took approximately 1 hour for the sample to reach thermal equilibrium with the environment.

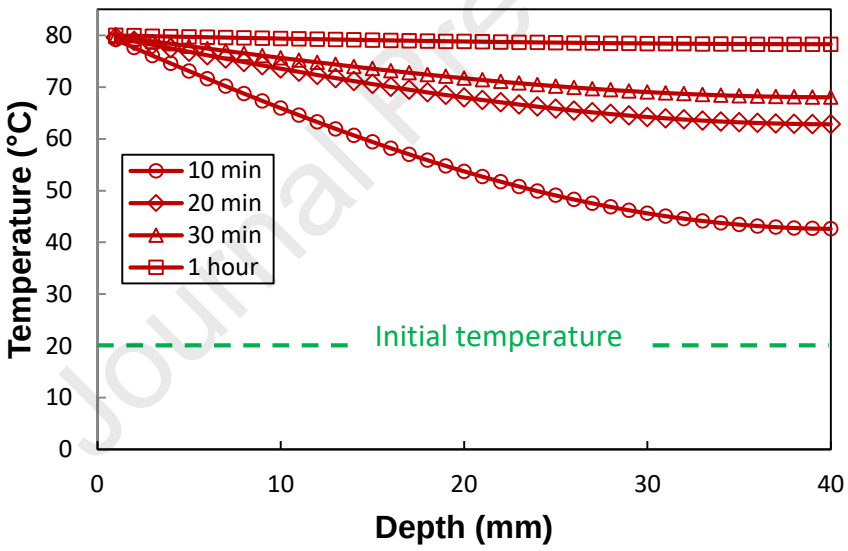

Figure 11: Evolution of the mortar temperature stored at 80°C

The tests were conducted at temperatures below 100°C and 65% relative humidity. The results and conclusion that higher temperatures accelerate carbonation are valid only under these specific test conditions. Wang et al [26] performed carbonation tests on different Portland cement pastes, some initially saturated and others totally dry. The tests lasted 1 hour and covered a temperature range of 20-300°C without controlling relative humidity. Initially dry samples showed minimal carbonation, while initially saturated samples exhibited an increase in carbonation rate between 20 and 100°C, followed by a decrease between 100 and 300°C. These results emphasize the role of water in the carbonation process. For initially dry samples,

carbonation could not occur due to the unavailability of water, which is the reaction medium. In the case of initially saturated samples, an optimal temperature for carbonation exists, where the effects of decreasing hydrate and CO_2 solubility, along with water saturation in the material, become more significant than the acceleration of diffusion processes in the aqueous and gas phases. Maintaining a minimum moisture level is essential for CO_2 dissolution and carbonation reactions. Above 100°C and without controlling relative humidity, all liquid water evaporates rapidly from the samples, leaving insufficient time for the reaction to take place. In other words, carbonation tends to decrease as the water content becomes insufficient for chemical reactions. Therefore, the effect of temperature is strongly dependent on humidity. To understand the concept of the optimum temperature for the carbonation process, it is crucial to consider the influence of relative humidity.

4.2 Numerical results

4.2.1 Calibration of the characteristic times of the reaction of dissolution of $Ca(OH)_2$ and carbonation of CSH

The carbonation model detailed in section 2 requires the calibration of the characteristic times τ_{CH} and τ_{CSH} at the two studied temperatures. The table below provides an overview of the input parameters used for the characteristic times calibration simulations.

Table 4: Input parameters used for the calibration of characteristic times

	Input	Value
External environment	% CO_2	15
	RH (%)	65
	Temperature (°C)	20°C / 80°C
Material	Porosity (%)	22
	$n^0_{Ca(OH)2}$ (mol/L)	1.300
	n^0_{CSH} (mol/L)	1.061
	n^0_{CaCO3}(mol/L)	0
	Sorption-desorption isotherm	Experimental results determined by DVS (4.1.3)
	W (%)	At 20°C: 3.5 At 80°C: 2
	Initial temperature (°C)	20

The calibration was performed by analyzing the time-evolution of the mineralogical composition (evolution of the amount of remaining portlandite and precipitated calcium carbonate) of the sample taken at depth 1 with a thickness of 1.3 cm (Figure 12 and Figure 13). The amount of carbonated CSH (experimental value) is calculated from the amount of portlandite and precipitated calcium carbonate determined by TGA.

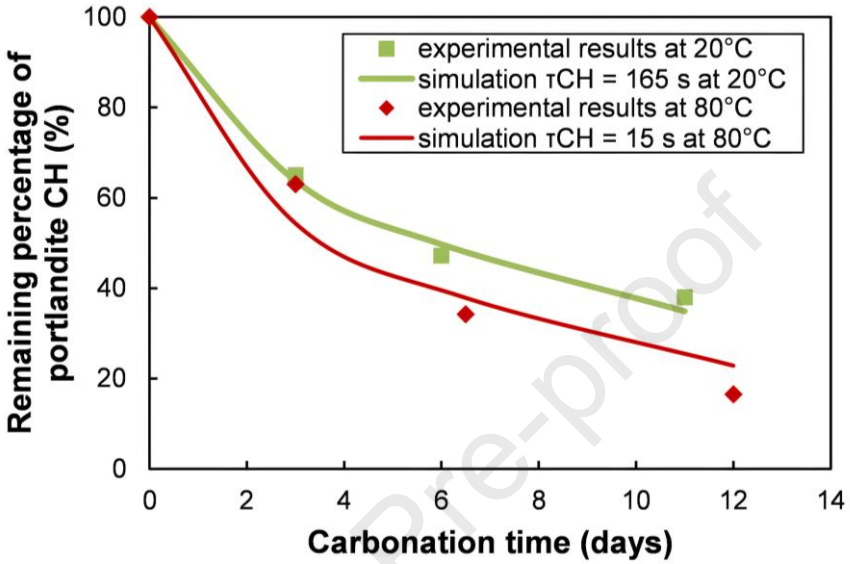

Figure 12: Remaining portlandite content CH of samples taken at depth 1 during carbonation at 20°C and 80°C

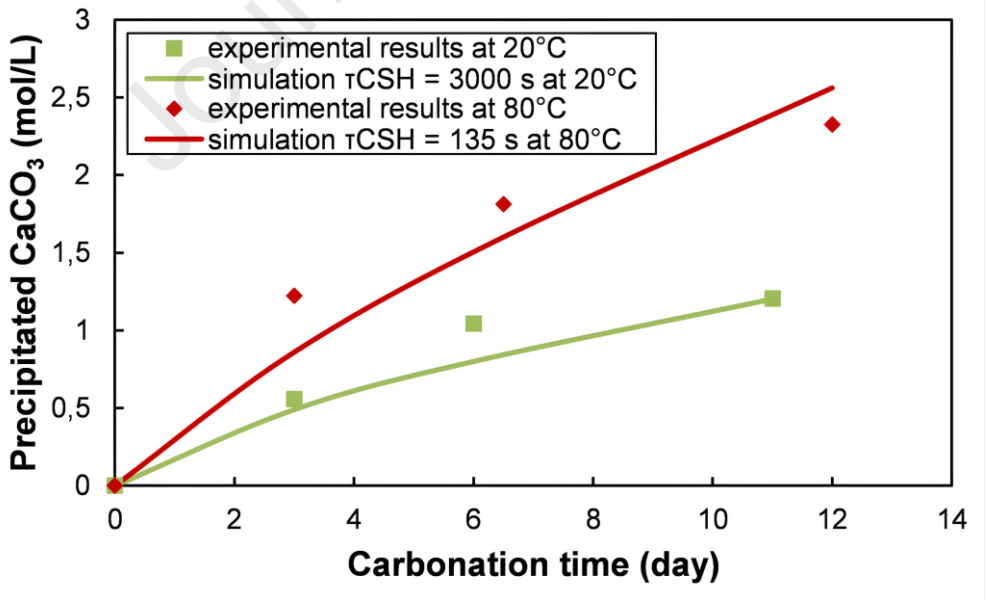

Figure 13: Precipitated calcium carbonate content of samples taken at depth 1 during carbonation at 20°C and 80°C

Based on these results and using inverse analysis, the evaluation of these two characteristic times was performed by dichotomy. Inverse analysis involves iteratively adjusting model

parameters until the simulated results match the observed experimental data. In the case of evaluating characteristic times associated with carbonation processes, dichotomy is a method commonly used to converge efficiently on optimal parameter values. Based on the evolution of the remaining percentage of portlandite determined by TGA (Figure 12), τ_{CH} was calibrated at 165 ± 15 s and 15 ± 3 s at 20°C and 80°C respectively. Once τ_{CH} calibrated, it was used with the amount of $CaCO_3$ formed and determined experimentally by TGA (Figure 13) to calibrate (by dichotomy) the characteristic time of carbonation of CSH. τ_{CSH} was calibrated at 3000 ± 300 s and 135 ± 15 s respectively at 20°C and 80°C. This calibration shows that chemical kinetics are faster at higher temperature, since characteristic times are lower at 80°C than at 20°C.

4.2.2 Simulation of carbonation at 20°C and 80°C

After calibrating the characteristic times for carbonation at 20°C and 80°C, the model can be used to analyze the effects of the carbonation of studied material at these two temperatures. It is noteworthy that the model was calibrated and validated using CEM I Portland cement-based materials, thus characteristic times could be different for other binders and materials. The spatio-temporal evolution of the amount of CO_2 bound by the mortar can then be deduced from the amount of $CaCO_3$ precipitated.

Figure 14 shows the evolution of porosity of the 4 cm samples, from both experimental and numerical data, during carbonation at 20°C and 80°C. As expected, the decrease in porosity is faster at 80°C than 20°C, as carbonation is promoted by increasing the temperature to 80°C for a relative humidity value of 65% as shown by the results of mineralogical evolution and carbonation depths in the previous section. In addition, a rather good correlation between the experimental and numerical results can be observed. It should be noted that coupled THC models require various input parameters, including material properties, environmental conditions, and reaction kinetics. Obtaining precise data for model calibration is challenging, particularly for complex cementitious materials . For instance, parameters such as τ_{CH} and τ_{CSH} may only be determined at specific temperatures, such as 80°C. Testing the model at different temperatures requires additional experimental tests for accurate parameter determination. Calibration may also demand experimental data that are not always readily available. Additionally, model validation requires further experiments, such as testing different mixtures with varied water-to-cement ratios, and comparing their carbonation behavior to model predictions.

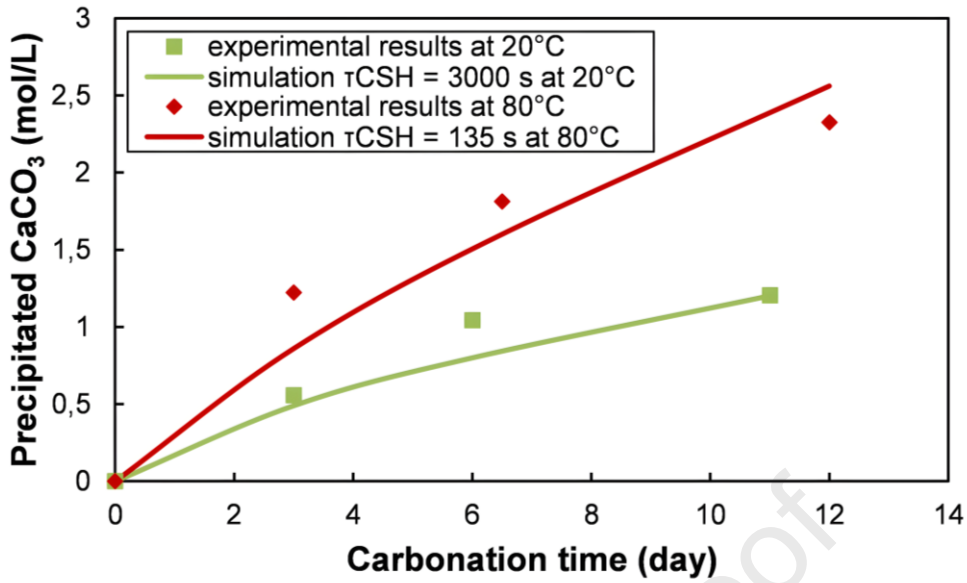

669

670 **Figure 14: Evolution of porosity of samples taken at depth 1 during carbonation at 20°C and**
671 **80°C**

672 Figure 15 and Figure 16 show the spatio-temporal evolution of the amounts of portlandite and
673 calcium carbonate during carbonation at 20°C and 80°C, respectively. The comparison between
674 the diagrams obtained at 20°C and those obtained at 80°C shows that carbonation is faster at
675 80°C, as observed from the experimental results. A a given time and given depth, the quantity
676 of remaining portlandite is lower and the quantity of precipitated calcite is higher. After 12 days
677 of carbonation, the amount of precipitated calcite reaches 2.5 mol/l at 80°C while it remains
678 close to 1.5 mol/l at 20°C.

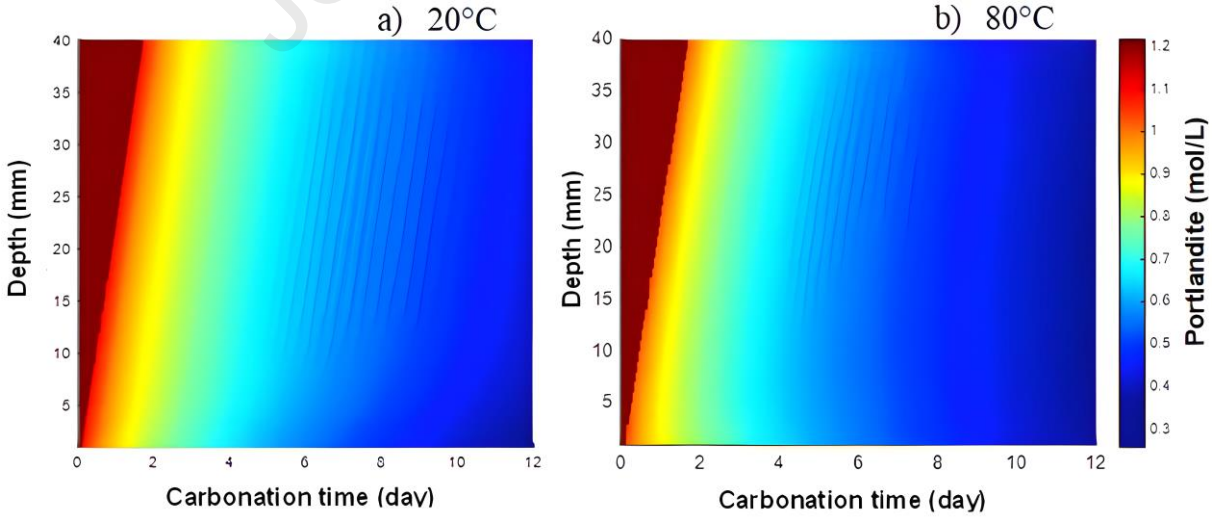

679

680 **Figure 15: Spatio-temporal evolution of the amount of portlandite remaining during**
681 **carbonation at a) 20°C and b) 80°C**

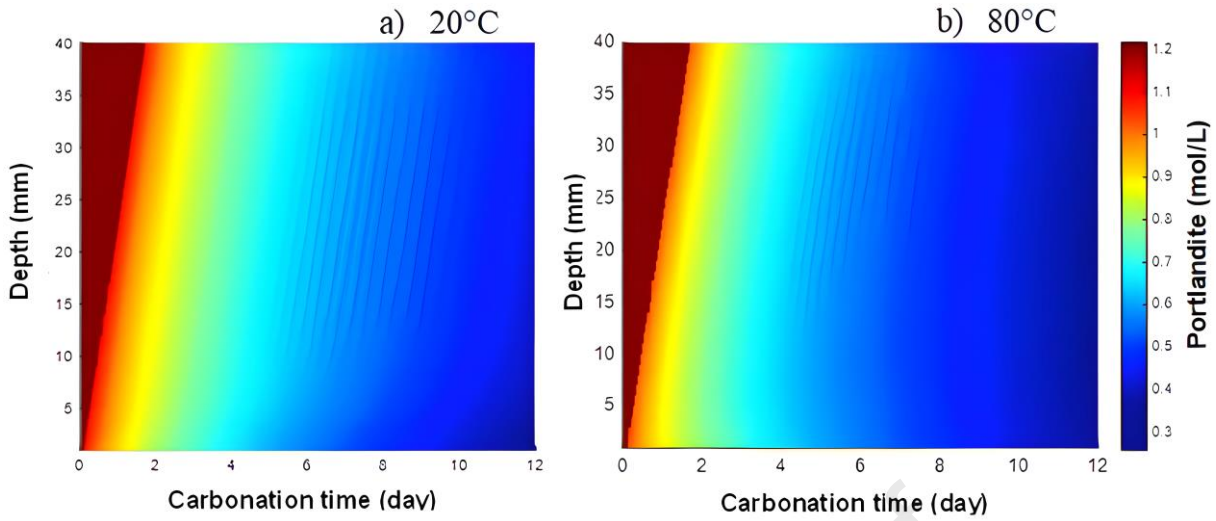

682

683 **Figure 16: Spatio-temporal evolution of the amount of precipitated calcium carbonate during**
684 **carbonation at a) 20°C and b) 80°C**

685 These quantities can be measured experimentally, but the experimental measurements are
686 discontinuous, whereas this model provides a continuous spatiotemporal evolution of these
687 parameters. Some parameters are difficult to evaluate and quantify experimentally, such as the
688 amount of carbonated CSH [17], the evolution of temperature, and the evolution of the hydric
689 state, all of which can be provided by the model.

690 ### 4.2.3 Simulation of the influence of both temperature and initial water
691 ### content on CO_2 uptake

692 The effects of temperature and relative humidity on carbonation are strongly coupled. The
693 samples used in this study were stored in an air-conditioned room for almost a year before
694 accelerated carbonation in order to be more representative of recycled aggregates mortar. The
695 tested samples were thus nearly in equilibrium with the carbonation environment, i.e., 20°C and
696 65% RH. Furthermore, this preconditioning time allows the mortar to age and ensures
697 significant natural carbonation, making it more representative of the mortar in RCA. The effect
698 of temperature on the evolution of the mortar water saturation and the effect of the initial water
699 saturation of mortar on carbonation kinetics and CO_2 storage were not examined in the
700 simulations presented above. Thus, in order to study the effect of temperature on the evolution
701 of these parameters, simulations were performed by varying the initial water saturation. If this
702 model proves to be sensitive to the effect of temperature on water transfer and thus on
703 carbonation, it will be useful to determine the initial saturation degree of RCA necessary to
704 optimize their carbonation.

In this section, simulations were performed on the same cementitious material and under the same environmental conditions in terms of temperature (20°C and 80°C), relative humidity (65%) and percentage of carbon dioxide (15%). The initial water saturation of the mortar was the only parameter changed. Figure 17 shows the evolution of the amount of carbon dioxide stored in the mortar after its carbonation for 24 hours as a function of the initial saturation degree of the mortar. A first observation shows that whatever the initial saturation degree of the mortar, the carbonation curve at 20°C is always lower than the carbonation curve at 80°C. It is noteworthy that the external relative humidity is controlled at 65%. Under these conditions, an increase in temperature from 20°C to 80°C accelerates the carbonation whatever the initial saturation level of the mortar. In other words, even if the initial optimal hydric state of the cementitious material is ensured at 20°C and not at 80°C, carbonation is favored at 80°C for an external humidity of 65%.

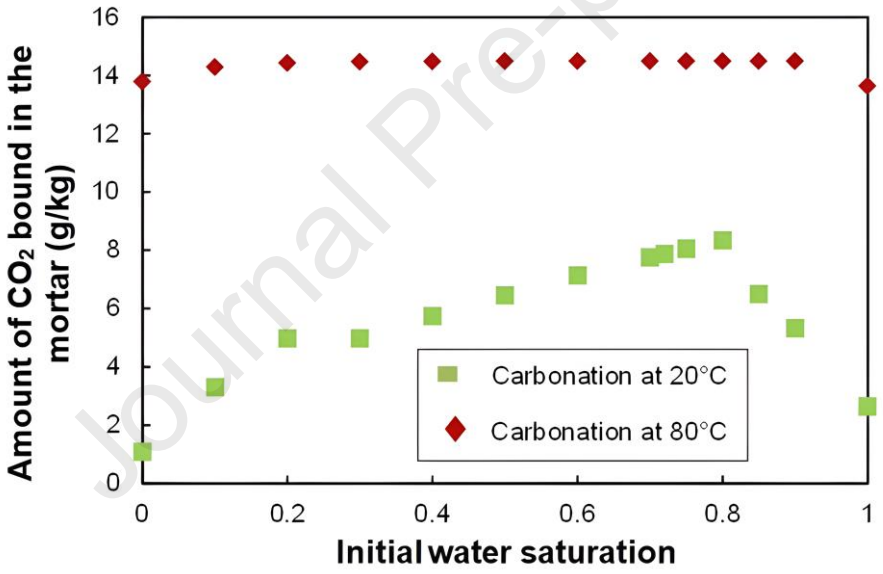

Figure 17: Evolution of the quantity of carbon dioxide precipitated during 24 hours of carbonation at 20°C and 80°C

Figure 17 also shows that the shape of the curve at 20°C is different from carbonation at 80°C: a peak is clearly visible at 20°C for an initial saturation degree of the mortar around 0.8 [63]. According to the sorption-desorption curves presented in Figure 9 and Figure 10, a relative humidity of 65% corresponds to a water saturation degree of 0.47 at 20°C and 0.25 at 80°C. Figure 18 shows the evolution of the saturation degree in the initially saturated mortar during 24 hours of carbonation at 20°C and 80°C respectively. It seems that for the carbonated sample at 20°C, the equilibrium water content has not been reached yet. After 24 hours of carbonation, the sample is still at relatively high water saturation, whereas at 80°C less than 10 hours were

necessary for the saturated mortar to reach a water saturation profile close to the equilibrium with the external environment. Therefore, these findings illustrate how this model facilitates the determination of the optimal initial water saturation level for the cementitious material at both 20°C and 80°C, aiming to optimize carbonation under specific temperature and relative humidity conditions.

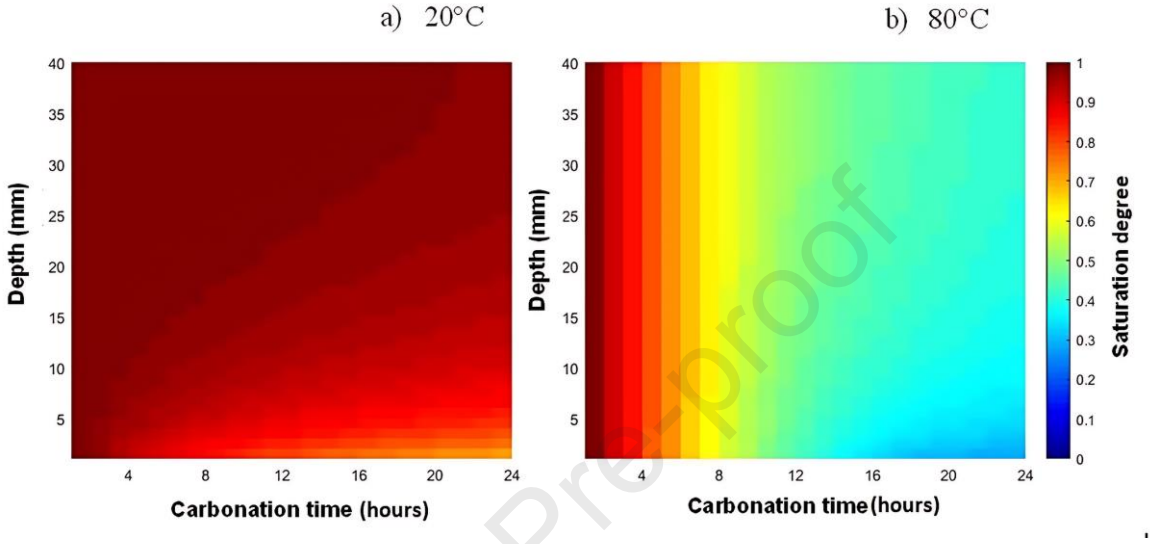

Figure 18: Spatio-temporal evolution of saturation degree during 24-hour carbonation at a) 20°C and b) 80°C

5 Conclusion

The use of hot and wet gases from cement plants has been suggested to accelerate the carbonation of recycled concrete aggregates (Carbon Capture and Utilization (CCU) methods). The effect of temperature increase on the kinetics and mechanisms of accelerated carbonation is investigated in this experimental and numerical study. Two temperatures (20°C and 80°C) were considered, with a controlled relative humidity of 65%.

The experimental results show that increasing the temperature from 20°C to 80°C with a relative humidity of 65% accelerates the carbonation rate by 62%. Thermally activated diffusive transport of carbon dioxide as well as accelerated reaction kinetics are the predominant factors compared to the retrograde solubility of portlandite, CSH, and carbon dioxide in this temperature range. Temperature also significantly modifies the sorption-desorption isotherms. In agreement with the literature, the general shape of the isotherm is altered, the equilibrium water content is significantly reduced at 80 °C over the entire relative humidity range, and the water content for high saturation rates at 80 °C was significantly lower than that at 20 °C.

A numerical model is developed to simulate accelerated carbonation of cementitious materials at 80°C, considering heat transfer, temperature's influence on water transfer and dissolution, and carbonation of carbonatable hydrates. This coupled thermo-hydro-chemical modeling enhances our understanding of carbonation mechanisms by considering temperature, moisture, and chemical reactions. It cen be used to develop industrial strategies to reduce CO_2 emissions and enhance environmental sustainability of cement-based materials. Experimental data calibrate two model parameters, validating results. The model describes temperature and mortar saturation evolution under various carbonation conditions and predicts remaining CSH, portlandite, and precipitated calcium carbonate and CO_2 storage during carbonation at 20°C and 80°C. It also estimates optimal initial water saturation degrees. CO_2 binding via carbonation hinges on factors like relative humidity, CO_2 levels, and saturation rate, [64] highlighting the importance of predicting these effects for cost-effective CO_2 capture.

The literature review and the experimental and numerical results show that the effect of temperature is strongly linked to the surrounding relative humidity and the saturation degree. Specifying an optimal temperature for the carbonation process should be associated with information on the control of external relative humidity. Given that this study focuses on a specific relative humidity level, future research should explore optimizing temperature settings while considering external relative humidity control. Additionally, it is crucial to study the effects of other potentially influential factors such as gas flow rate, CO_2 concentration, and the initial moisture content of the RCA. Investigating these additional variables could provide a more comprehensive understanding of the process. Furthermore, examining alternative compositions and various types of cements would be beneficial for validating the practicality and effectiveness of the model developed in this study. Collectively, these results could serve as a valuable database for AI systems aimed at optimizing the process. Moreover, incorporating the influence of CO_2 concentration and integrating this model within a "process engineering" approach would further enhance the robustness and applicability of the findings.

Acknowledgements

The French national research agency (ANR) is gratefully acknowledged for supporting CO_2NCRETE Project.

6 References

[1] D. Xuan, "Assessment of mechanical properties of concrete incorporating carbonated recycled concrete aggregates," *Cem. Concr. Compos.*, p. 8, 2016.

[2] J. Zhang, C. Shi, Y. Li, X. Pan, C.-S. Poon, and Z. Xie, "Influence of carbonated recycled concrete aggregate on properties of cement mortar," *Constr. Build. Mater.*, vol. 98, pp. 1–7, Nov. 2015, doi: 10.1016/j.conbuildmat.2015.08.087.

[3] C.-S. Poon and D. Chan, "The use of recycled aggregate in concrete in Hong Kong," p. 13, 2007.

[4] C. S. Poon, Z. H. Shui, and L. Lam, "Effect of microstructure of ITZ on compressive strength of concrete prepared with recycled aggregates," *Constr. Build. Mater.*, vol. 18, no. 6, pp. 461–468, Jul. 2004, doi: 10.1016/j.conbuildmat.2004.03.005.

[5] M. Surendar, G. Beulah Gnana Ananthi, M. Sharaniya, M. S. Deepak, and T. V. Soundarya, "Mechanical properties of concrete with recycled aggregate and M−sand," *Mater. Today Proc.*, vol. 44, pp. 1723–1730, 2021, doi: 10.1016/j.matpr.2020.11.896.

[6] C. S. Poon, P. Shen, Y. Jiang, Z. Ma, and D. Xuan, "Total recycling of concrete waste using accelerated carbonation: A review," *Cem. Concr. Res.*, vol. 173, p. 107284, Nov. 2023, doi: 10.1016/j.cemconres.2023.107284.

[7] Z. Maciej, I. Maruyama, A. Iizuka, and J. Skibsted, "Enforced carbonation of cementitious materials," *Cem. Concr. Res.*, vol. 174, p. 107285, Aug. 2023, doi: 10.1016/j.cemconres.2023.107285.

[8] B. Zhan, C. S. Poon, Q. Liu, S. Kou, and C. Shi, "Experimental study on CO2 curing for enhancement of recycled aggregate properties," *Constr. Build. Mater.*, vol. 67, pp. 3–7, Sep. 2014, doi: 10.1016/j.conbuildmat.2013.09.008.

[9] S.-C. Kou, B. Zhan, and C.-S. Poon, "Use of a CO2 curing step to improve the properties of concrete prepared with recycled aggregates," *Cem. Concr. Compos.*, vol. 45, pp. 22–28, Jan. 2014, doi: 10.1016/j.cemconcomp.2013.09.008.

[10] J. M. Torrenti *et al.*, "The FastCarb project: Taking advantage of the accelerated carbonation of recycled concrete aggregates," *Case Stud. Constr. Mater.*, vol. 17, p. e01349, Dec. 2022, doi: 10.1016/j.cscm.2022.e01349.

[11] H. Zhang, S. Cao, and E. Yilmaz, “Carbon nanotube reinforced cementitious tailings composites: Links to mechanical and microstructural characteristics,” *Constr. Build. Mater.*, vol. 365, p. 130123, Feb. 2023, doi: 10.1016/j.conbuildmat.2022.130123.

[12] J. Skocek, M. Zajac, and M. Ben Haha, “Carbon Capture and Utilization by mineralization of cement pastes derived from recycled concrete,” *Sci. Rep.*, vol. 10, no. 1, p. 5614, Mar. 2020, doi: 10.1038/s41598-020-62503-z.

[13] N. Lippiatt, T.-C. Ling, and S.-Y. Pan, “Towards carbon-neutral construction materials: Carbonation of cement-based materials and the future perspective,” *J. Build. Eng.*, vol. 28, p. 101062, Mar. 2020, doi: 10.1016/j.jobe.2019.101062.

[14] C. Pade and M. Guimaraes, “The CO2 uptake of concrete in a 100 year perspective,” *Cem. Concr. Res.*, p. 9, 2007.

[15] J. G. Jang, G. M. Kim, H.-G. Kim, and H. K. Lee, “Review on recent advances in CO2 utilization and sequestration technologies in cement-based materials,” *Constr. Build. Mater.*, vol. 127, pp. 762–773, 2016.

[16] E. Drouet, S. Poyet, and J.-M. Torrenti, “Temperature influence on water transport in hardened cement pastes,” *Cem. Concr. Res.*, vol. 76, pp. 37–50, Oct. 2015, doi: 10.1016/j.cemconres.2015.05.002.

[17] E. Drouet, “Impact de la température sur la carbonatation des matériaux cimentaires: prise en compte des transferts hydriques,” p. 314.

[18] M. Sereng, “Amélioration des propriétés des granulats recyclés par stockage de CO2 : étude de la faisabilité préindustrielle,” Université Paris-Est, 2020.

[19] M. Fernandezbertos, S. Simons, C. Hills, and P. Carey, “A review of accelerated carbonation technology in the treatment of cement-based materials and sequestration of CO2,” *J. Hazard. Mater.*, vol. 112, no. 3, pp. 193–205, Aug. 2004, doi: 10.1016/j.jhazmat.2004.04.019.

[20] Mori, T., Shirayamaka, K, and Yoda, A, “Carbonation of blast-furnace cement,” *Poceedingd of the 26th annual meeting of cement association of Japan 326-329*, 1972.

[21] Yanagi, K and Tomosawa, F, "An experiment onb the prediction of carbonating speed of concrete. Part II: influence of various factors on carbonation," *Proceedings of Architectural Institute of Japan A(1124) : 247-248*, 1987.

[22] "Fundamental Modeling and Experimental Investigation of Concrete Carbonation," *ACI Mater. J.*, vol. 88, no. 4, 1991, doi: 10.14359/1863.

[23] Villain, G, Croquette, G, and Ounoughi, K, "Transferts dans les bétons et durabilités des ouvrages. Optimisation des conditions d'essais pour la carbonatation accélérée des bétons," Bordeaux, 2000.

[24] T. DHEILLY, R J., "Etude du systeme CaO-H2O-CO2 pour un stockage optimal de la chaux," *Ciments, bétons, platres, chaux*.

[25] L. Liu, J. Ha, T. Hashida, and S. Teramura, "Development of a CO2 solidification method for recycling autoclaved lightweight concrete waste," p. 4.

[26] D. Wang, T. Noguchi, T. Nozaki, and Y. Higo, "Investigation of the carbonation performance of cement-based materials under high temperatures," *Constr. Build. Mater.*, vol. 272, p. 121634, Feb. 2021, doi: 10.1016/j.conbuildmat.2020.121634.

[27] D. Wang, T. Noguchi, and T. Nozaki, "Increasing efficiency of carbon dioxide sequestration through high temperature carbonation of cement-based materials," *J. Clean. Prod.*, vol. 238, p. 117980, Nov. 2019, doi: 10.1016/j.jclepro.2019.117980.

[28] Thiery, "Modélisation de la carbonatation atmosphérique des matériaux cimentaires : Prise en compte des effets cinétiques et des modifications microstructurales et hydriques," p. 348, 2007.

[29] B. Bary and A. Sellier, "Coupled moisture—carbon dioxide–calcium transfer model for carbonation of concrete," *Cem. Concr. Res.*, vol. 34, no. 10, pp. 1859–1872, Oct. 2004, doi: 10.1016/j.cemconres.2004.01.025.

[30] M. Achour, "Modélisation du couplage carbonatation – chlorures et étude multiéchelle de l'influence des granulats sur la diffusivité dans les bétons," École centrale de Nantes, 2018.

[31] E. Samson and J. Marchand, "Modeling the effect of temperature on ionic transport in cementitious materials," *Cem. Concr. Res.*, vol. 37, no. 3, pp. 455–468, Mar. 2007, doi: 10.1016/j.cemconres.2006.11.008.

[32] E. Bastidas-Arteaga, A. Chateauneuf, M. Sánchez-Silva, Ph. Bressolette, and F. Schoefs, "Influence of weather and global warming in chloride ingress into concrete: A stochastic approach," *Struct. Saf.*, vol. 32, no. 4, pp. 238–249, Jul. 2010, doi: 10.1016/j.strusafe.2010.03.002.

[33] P. T. Nguyen, "Étude multiphysique du transfert de chlorures dans les bétons insaturés: prédiction de l'initiation de la corrosion des aciers," p. 229.

[34] V. G. Papadakis, "Effect of fly ash on Portland cement systems Part I. Low-calcium fly ash," *Cem. Concr. Res.*, p. 10, 1999.

[35] S. Talukdar, N. Banthia, and J. R. Grace, "Carbonation in concrete infrastructure in the context of global climate change – Part 1: Experimental results and model development," *Cem. Concr. Compos.*, vol. 34, no. 8, pp. 924–930, Sep. 2012, doi: 10.1016/j.cemconcomp.2012.04.011.

[36] G. Grasa, R. Murillo, M. Alonso, and J. C. Abanades, "Application of the random pore model to the carbonation cyclic reaction," *AIChE J.*, vol. 55, no. 5, pp. 1246–1255, May 2009, doi: 10.1002/aic.11746.

[37] A. Scaltsoyiannes, A. Antzaras, G. Koilaridis, and A. Lemonidou, "Towards a generalized carbonation kinetic model for CaO-based materials using a modified random pore model," *Chem. Eng. J.*, vol. 407, p. 127207, Mar. 2021, doi: 10.1016/j.cej.2020.127207.

[38] F. L. Smith and A. H. Harvey, "Avoid Common Pitfalls When Using Henry's Law," *Environ. Manage.*, p. 7.

[39] R. Sander, "Compilation of Henry's law constants (version 4.0) for water as solvent," *Atmospheric Chem. Phys.*, vol. 15, no. 8, pp. 4399–4981, Apr. 2015, doi: 10.5194/acp-15-4399-2015.

[40] M. Thiery, "Exemple d'application d'un modèle de carbonatation in situ," *BLPC • n°270-27*, p. 22, 2007.

[41] C. L. Dickson and D. R. M. Brew, "Solubilities of CaO–SiO2–H2O phases at 25°, 55° and 85°C," *Advances in cement research*.

[42] R. E. Hachem, "Etude multi-critères de la degradation des matériaux cimentaires par l'attaque sulfatique externe," p. 193.

[43] Charles EYRAUD, Armand ACCARY, “Analyses thermique et calorimétrique différentielles,” *Tech. Ing.*.

[44] M. Khachani, A. E. Hamidi, M. Halim, and S. Arsalane, “Non-isothermal kinetic and thermodynamic studies of the dehydroxylation process of synthetic calcium hydroxide Ca(OH)2,” p. 11, 2014.

[45] G. Villain, M. Thiery, and G. Platret, “Measurement methods of carbonation profiles in concrete: Thermogravimetry, chemical analysis and gammadensimetry,” *Cem. Concr. Res.*, vol. 37, no. 8, pp. 1182–1192, Aug. 2007, doi: 10.1016/j.cemconres.2007.04.015.

[46] A. Morandeau, M. Thiéry, and P. Dangla, “Investigation of the carbonation mechanism of CH and C-S-H in terms of kinetics, microstructure changes and moisture properties,” *Cem. Concr. Res.*, vol. 56, pp. 153–170, Feb. 2014, doi: 10.1016/j.cemconres.2013.11.015.

[47] S. T. Pham, “Modifications on Microporosity and Physical Properties of Cement Mortar Caused by Carbonation: Comparison of Experimental Methods,” *Adv. Mater. Sci. Eng.*, p. 10.

[48] Glasser, F.P., Pedersen, J., Goldthorpe, K., & Atkins, M.P., “Solubility reactions of cement components with NaCl solutions: I. Ca(OH) 2 and C-S-H. Advances in Cement Research, 17, 57-64.,” 2005.

[49] V. Shah and S. Bishnoi, “Carbonation resistance of cements containing supplementary cementitious materials and its relation to various parameters of concrete,” *Constr. Build. Mater.*, vol. 178, pp. 219–232, Jul. 2018, doi: 10.1016/j.conbuildmat.2018.05.162.

[50] R. He, “A Study on Carbonation for Low Calcium Fly Ash Concrete under Different Temperature and Relative Humidity,” vol. 15, p. 7.

[51] F. Brue, “Rôles de la température et de la composition sur le couplage thermo-hydro-mécanique des bétons,” p. 295.

[52] F. Kaddah, E. Roziere, H. Ranaivomanana, and O. Amiri, “Complementary use of thermogravimetric analysis and oven to assess the composition and bound CO2 content of recycled concrete aggregates,” *Dev. Built Environ.*, vol. 15, p. 100184, Oct. 2023, doi: 10.1016/j.dibe.2023.100184.

[53] Y. Li *et al.*, "Carbonation of the synthetic calcium silicate hydrate (C-S-H) under different concentrations of CO2: Chemical phases analysis and kinetics," *J. CO2 Util.*, vol. 35, pp. 303–313, Jan. 2020, doi: 10.1016/j.jcou.2019.10.001.

[54] J. Grandet, "Contribution à l'etude de la prise et de la carbonatation des mortiers au contact des matériaux poreux."

[55] F. Kaddah, H. Ranaivomanana, O. Amiri, and E. Rozière, "Accelerated carbonation of recycled concrete aggregates: Investigation on the microstructure and transport properties at cement paste and mortar scales," *J. CO2 Util.*, vol. 57, p. 101885, Mar. 2022, doi: 10.1016/j.jcou.2022.101885.

[56] M. Auroy, "Impact de la carbonatation sur les propriétés de transport d'eau des matériaux cimentaires," p. 288.

[57] S. T. Pham, "Modifications in Water Sorption Isotherms of Cement Mortars Caused by Carbonation: Effects of Cycles," *Adv. Mater. Res.*, vol. 1042, pp. 3–9, Oct. 2014, doi: 10.4028/www.scientific.net/AMR.1042.3.

[58] H. Ranaivomanana, "Transferts dans les milieux poreux réactifs non saturés : application à la cicatrisation de fissure dans les matériaux cimentaires par carbonatation." 2010.

[59] S. Poyet, "Experimental investigation of the effect of temperature on the first desorption isotherm of concrete," *Cem. Concr. Res.*, vol. 39, no. 11, pp. 1052–1059, Nov. 2009, doi: 10.1016/j.cemconres.2009.06.019.

[60] S. D. Pont, "Coupling between permeability and damage in concrete," p. 223.

[61] D. Kong, T. Lei, J. Zheng, C. Ma, J. Jiang, and J. Jiang, "Effect and mechanism of surface-coating pozzalanics materials around aggregate on properties and ITZ microstructure of recycled aggregate concrete," *Constr. Build. Mater.*, p. 8, 2010.

[62] O. Kinnane, "Experimental investigation of thermal inertia properties in hemp-lime".

[63] P. Akpinar and I. D. Uwanuakwa, "Investigation of the parameters influencing progress of concrete carbonation depth by using artificial neural networks," *Mater. Constr.*, vol. 70, no. 337, p. 209, Jan. 2020, doi: 10.3989/mc.2020.02019.

947 [64] Q. Phung, A. Varzina, J. Perko, D. Jacques, N. Maes, and Ö. Cizer, "On the Effects of
948 Relative Humidity and CO2 Concentration on Carbonation of Cement Pastes," in *XV*
949 *International Conference on Durability of Building Materials and Components. eBook of*
950 *Proceedings*, CIMNE, 2020. doi: 10.23967/dbmc.2020.103.

951 [65] P. Zandifaez, E. Asadi Shamsabadi, A. Akbar Nezhad, H. Zhou, and D. Dias-da-Costa,
952 "AI-Assisted optimisation of green concrete mixes incorporating recycled concrete
953 aggregates," *Constr. Build. Mater.*, vol. 391, p. 131851, Aug. 2023, doi:
954 10.1016/j.conbuildmat.2023.131851.

955

Highlights

- Accelerated carbonation of cement mortar at 20°C and 80°C in controlled relative humidity conditions
- A new thermo-hydro-chemical coupled model of carbonation is presented
- Input data of the model experimentally assessed at 20°C and 80°C
- Numerical simulations on the influence of initial water saturation on bound CO_2 content

Declaration of interests

☒ The authors declare that they have no known competing financial interests or personal relationships that could have appeared to influence the work reported in this paper.

☐ The authors declare the following financial interests/personal relationships which may be considered as potential competing interests: